DEPARTMENT OF
PRIMARY INDUSTRIES

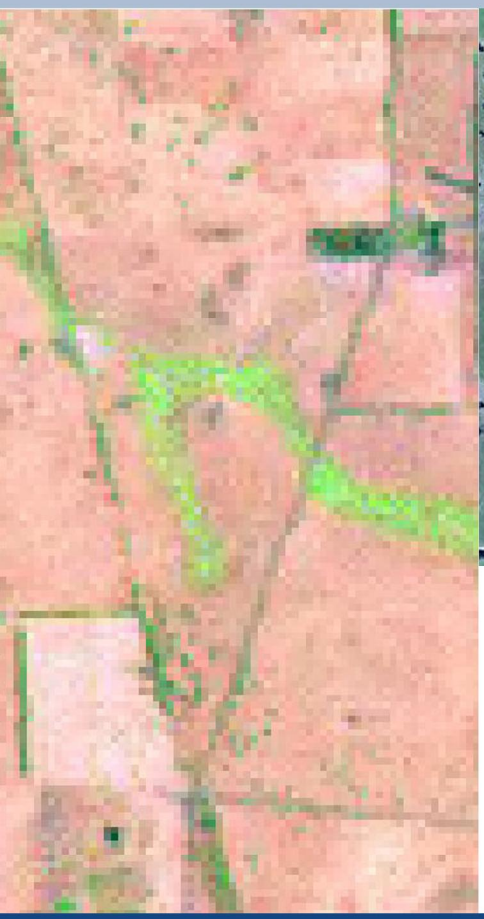

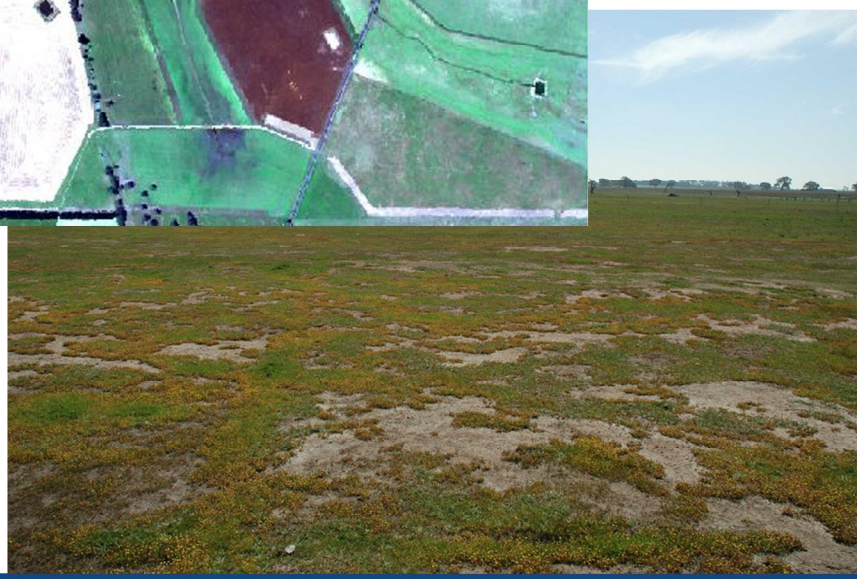

Mapping soil salinity using hyperspectral imagery

February 2007

Victoria
The Place To Be

Published by: Department of Primary Industries, 2007
Primary Industries Research Victoria
Bendigo
February 2007

Also published on http://www.dpi.vic.gov.au

Authorised by the Victorian Government, Midland Highway, Epsom, Victoria.
Printed by Latrobe Media Services, Bendigo.

The National Library of Australia Cataloguing-in-Publication entry:

Clark, R. M., 1955- .
Mapping soil salinity using hyperspectral imagery.

Bibliography.
ISBN 9781741990058 (pbk.).
1. Soil salinization – Remote-sensing maps. 2. Image processing – Digital techniques. 3. Spectrum analysis. I. Abuzar, Mohammad. II. Robinson, Nathan, 1975- . III. Victoria. Dept. of Primary Industries. IV. Title.

621.3678

Summary

This report summarises the work and findings of the project 'Mapping soil salinity using hyperspectral imagery'. The Agricultural Development Division (Department of Primary Industries) and the Department of Sustainability and Environment jointly funded the project.

This project is part of a body of work aimed at developing an operational methodology for mapping and monitoring soil salinity at a landscape scale. A cost-effective and accurate methodology would improve the Victorian Government's ability to implement, measure and report on the effectiveness of key Commonwealth and State Government policies. To achieve a fully operational methodology at a suitable scale, the following key scientific questions need be addressed:

1. Can we discriminate salt-tolerant vegetation from salt-sensitive vegetation based on their reflectance?
2. Can we discriminate between the target species under field conditions using airborne sensors where atmospheric conditions attenuate the reflectance signal?
3. Can we apply this solution at a landscape scale?
4. Could this methodology and technology be used to address other applications?

Previous work funded by the National Action Plan (NAP) demonstrated that it was possible to discriminate between salt-tolerant and salt-sensitive species based on reflectance. The current project demonstrates that it is possible to deal with atmospheric effects and map soil salinity accurately based on vegetation, using an airborne hyperspectral sensor with some qualifications. Whether it is technically feasible and economically viable to use this technology at its current level of development to provide a landscape scale solution requires further research to ensure that multiple hyperspectral swathes can be mosaiced into one single geometrically and radiometrically coherent image, and that it is possible to deal efficiently with the large volume of data that this approach would generate. One means of improving the economic viability of this approach is to develop a number of applications that could be addressed using the same dataset. A number of applications suggest themselves, specifically native grassland mapping and monitoring, weed mapping, vegetation and crop condition monitoring, revegetation monitoring and soil mapping.

This investigation examined the potential to map soil salinity using airborne hyperspectral imagery. To this end, the research applied a range of image analysis techniques and methods for collecting reference spectra for mapping soil salinity using hyperspectral data and examined the effect of varying the spatial resolution of the hyperspectral data. Significant results were achieved, with several techniques producing accuracies around 80% for mapping the extent of salt affected soil. The best algorithm produced an accuracy of 85% for mapping saline soil, 92% for non-saline soil with an overall accuracy of 89%.

This report records the accuracy attained by each combination of classification algorithms and reference spectra as well as the accuracy attained using different spatial resolutions for the hyperspectral image data. It discusses the strengths and weaknesses of the various classification algorithms and methods for generating reference spectra and documents a preferred methodology for mapping the extent of soil salinity using hyperspectral data. It also comments on current limitations of hyperspectral data and associated analytical techniques, the appropriate spatial resolution for mapping soil salinity and other potential applications based on the results and a review of related literature. In the course of this project, several issues that currently limit the implementation of this technology at a larger scale were identified, the prime impediment being the ability to calibrate individual airborne hyperspectral swathes to allow mosaicing of multiple swathes into a single coherent image. This step is essential for landscape scale applications while hyperspectral imagery is captured from an airborne rather than satellite platform. In the interests of achieving the primary aim of this project (to investigate the potential to map soil salinity using hyperspectral imagery) within the resources of the project, these issues were not pursued, but are raised in the discussion section.

This study was conducted in an agricultural landscape just north of Hamilton in Victoria's Western District. Soil salinity levels in the study area were not extreme and the saline sites tend to be characterised by a good cover of salt-tolerant vegetation (mainly annual grasses and herbs), the absence of salt-sensitive vegetation and relatively little bare soil. This level of salinity and related surficial expression is common across much of Victoria, particularly where annual rainfall exceeds 400 mm and evaporation rates are not extreme. It is a

difficult environment in which to employ a remote sensing approach, as there is relatively little contrast between the saline and non-saline areas in terms of broad vegetation type and cover. In comparison previous studies tended to be located in high to extreme saline environments typically dominated by extensive bare, salt scalded areas and perennial halophytic vegetation. In such environments there is generally a greater degree of contrast between the saline and non-saline areas, which is more favourable to a remote sensing approach. If we are to develop a remote sensing tool for monitoring soil salinity it is important that it is effective and reliable across all of the major saline environments common in Victoria.

This study used HyMap hyperspectral imagery with 125 spectral bands (bandwidth 10–20 nm) and 3 m pixels, employing both whole pixel and sub-pixel classification techniques to map salt affected soil. Classification was based on the observed correlation of salt affected soil with the presence of salt-tolerant species and the absence of salt-sensitive species rather than directly mapping saline soil. Reference spectra were derived from the image data based on either image specific spectral properties (endmembers) or training areas located in the field using a GPS instrument. Reflectance measurements for 15 salt-tolerant and salt-sensitive plant species common to the area made using artificial lighting in the laboratory were also used as reference spectra. Soils in the study area were sampled and analysed to characterise their physical properties and chemical composition. X-ray Diffraction (XRD) analysis was used to determine the clay mineralogy of samples, but little visible correlation was found between clay mineralogy and halites (NaCl), thus clay mineralogy was not considered to be a useful predictor of soil salinity levels for this study. Reflectance measurements were collected for both saline and non-saline soil samples under artificial lighting in the laboratory and used as reference spectra for the image analysis. To assess the accuracy of the image analyses, validation data was collected in the field to compare against the image classification. Validation sites were selected using a stratified random selection process applied to previous field salinity survey data. For the saline class, 111 points were located and verified in the field. For the non-saline class, 155 points were located and verified in the field. This number of validation points was more than sufficient to determine the accuracy of each assessment to a level of +/- 10% with 90% confidence. None of the validation sites were used as training data. Each nominated point was located in the field using a GPS and its salinity status confirmed or amended based on the standard vegetation based field assessment.

Results were good with several classification algorithms achieving accuracies over 80% +/- 10% (with 90% confidence) within a single image swathe. The best results were obtained using sub-pixel techniques, with a two-stage classification based on the Mixture Tuned Matched Filtering (MTMF) algorithm returning an overall accuracy (correct classification for both saline and non-saline classes divided by the number of samples) of 89% +/- 10% (with 90% confidence). This method also achieved a very good accuracy for each class individually with accuracies for saline soil of around 84% and non-saline soil around 93%. There is some potential to improve on the accuracy and detail achieved using this sub-pixel approach by undertaking a more detailed analysis of the land cover classes on a per pixel basis and application of a more sophisticated second stage classifier, but this requires further investigation. Such improvement may lead to reliable estimates of severity, but current classifications were limited to the extent of soil salinity.

The technical skills developed in this project provide a strong foundation to improve the application of hyperspectral data for mapping soil salinity and to investigate in detail some of the issues that currently make the application of this technology difficult at landscape scale. Mapping soil salinity is only one application that may benefit from the development of this technology. This project should be viewed as developing skills that could be utilised to map and monitor a number of critical biophysical and biochemical factors related to vegetation, soil and biodiversity.

Contents

Figures

Tables

Acknowledgments

The authors would like to acknowledge the following people for their contributions and support for this project:

Michael Blake	Landholder, Hamilton
Leigh Callinan	Department of Primary Industries, Bendigo
Phil Cook	Department of Primary Industries, Bendigo
Dr. Remy Dehaan	Charles Sturt University Wagga
Paul Daniel	CSIRO, Canberra
Bob Gannon	Landholder, Hamilton
Wayne Harvey	Department of Primary Industries, Bendigo
Peter Hayes	Landholder, Hamilton
Wendy McAllister	Department of Primary Industries, Tatura
Leisa Macartney	Clarity Editing Services, Woodend
Penny Riffkin	Department of Primary Industries, Hamilton
Melanie Robinson	Department of Primary Industries, Bendigo
Susanne Thulin	Department of Sustainability and Environment
Leon Woodhouse	RMIT, Melbourne

The authors would also like to gratefully acknowledge the joint funding provided by Department of Primary Industries—Agriculture Development Division (Victoria) and the Department of Sustainability and Environment—Land and Natural Resources (Victoria) that made this research possible.

List of abbreviations

AVIRIS	Airborne Visible/Infrared Imaging spectrometer
CGDL	Corporate Geospatial Data Library
CMA	Catchment Management Authority
DPI	Department of Primary Industries
DSE	Department of Sustainabilty and Environment
$EC_{1:5}$	Electrolytic conductivity from a 1:5 strength solution
EC_e	Electrolytic conductivity from saturated soil
EFFORT	Empirical Flat Field Optimal Reflectance Transformation
ETM+	Enhanced Thematic Mapper
FOV	field of view
GCP	ground control point
GPS	Global Positioning System
MF	matched filter
MNF	Minimum Noise Fraction
MSS	Multispectral Scanner
MTMF	mixture-tuned matched filtering
NAP	National Action Plan
PPI	Pixel Purity Index
SAM	Spectral Angle Mapper
SFF	Spectral Feature Fitting
SNR	signal to noise ratio
TM	Thematic Mapper
TSS	Total Soluble Salts
VNIR	Visible Near Infrared
XRD	Xray diffraction

Mapping soil salinity using hyperspectral imagery

R. Clark, M. Abuzar and N. Robinson

Keywords: [soil salinity, airborne hyperspectral image, reference spectra]

1 Introduction

Soil salinity is a hazard with severe consequences in both dry and irrigated areas (NLWRA 2000; Spies & Woodgate 2005). All remedial strategies to contain and mitigate the impact of soil salinity require that salinity is firstly detected and delineated at the appropriate scale. Remote sensing technologies using multispectral imagery have previously been used to map soil salinity (Al Saifi & Qari 1996; Dwivedi & Sreenivas 1998; Furby et al. 1995; Hill 1990) at different scales with varying degrees of success. Multispectral sensors generally measure reflectance at a few wide wavelength bands (typically >50 nm) separated by spectral segments where no measurements are taken and are usually limited to identifying broad categories of land cover or surface condition. This type of data is most successful at high to extreme levels of soil salinity, which are frequently dominated by extensive bare, salt scalded areas and perennial halophytic vegetation. In comparison, areas affected by low to moderate soil salinity levels are typically characterised by a good cover of salt-tolerant vegetation, an absence of salt-sensitive vegetation and little bare soil. Such areas are more difficult to map, as there is relatively little contrast between the saline and non-saline areas. Hyperspectral sensors with a large number of narrow (typically < 20 nm), contiguous bands are capable of providing sufficient information to identify and distinguish between spectrally similar but unique materials (Shippert 2004) and offer new opportunities to successfully map and monitor areas affected by low to moderate levels of soil salinity.

In field conditions, saline soils coexist with a variety of ground covers and vary considerably in composition, structure and colour. This situation causes large variations in reflectance (Ben-Dor, Irona & Epema. 1999; Zink 2001). Though salt tends to concentrate locally and create variable features of patchy nature (Metternicht & Zinck 2003), its surficial manifestation seems to be more 'variable' than 'unique'. It is therefore strategic that saline soils are studied by targeting their 'surrogates' which are spectrally discernible. One important surrogate is the affected vegetation (Dehaan & Taylor 2003, 2002; Schmidt & Skidmore 2003). This study has adopted a similar approach in identifying ground cover (vegetation included) as a surrogate of saline versus non-saline areas, and to explore 'similar' hyperspectral responses in a dryland agricultural region. Although the image analysis concentrated on detecting salt-tolerant and salt-sensitive vegetation as a surrogate for soil salinity, soils were sampled and analysed to develop an understanding of their contribution to reflectance data and to evaluate the ability to predict the difference between saline and non-saline exposed soils based on their reflectance spectra.

Hyperspectral images are analysed in a variety of ways (Metternicht & Zinck 2003; Schmidt 2003) in order to achieve the objectives of target detection and the mapping of surface properties (Shippert 2004). However, there are two broad approaches that encompass distinctively different methods. One is based on 'full pixel' analysis, which broadly includes techniques on data reduction, image transformation, image derivatives and regression. The second approach is based on 'sub-pixel' analysis that includes various methods of mixture modelling.

The resolution and contiguous nature of spectral measurements made by hyperspectral sensors enables *spectral matching* as an analytical method (Ben-Dor et al. 2003; Clark 1999). This reinforces the usefulness of spectral libraries as reference spectra in detecting and mapping materials considered likely to be present in an image (Ben-Dor, Iron & Epema 1999). However, the hyperspectral bands can be analysed as 'multivariate' datasets as well. Stepwise regression (Csillag, Pasztor & Biehl 1993) and correlation analysis are examples in this context. In some cases the objective can be to eliminate redundant information or to obtain optimum number of bands for analysis. For example, Bajcsy and Groves (2004) tested various techniques to arrive at a set of four to eight bands out of 120 bands in the range of 0.4 – 0.9 μm of airborne H-3 sensor in best predicting the electrical conductivity.

Data transformation generally derives a new set of information to replace the original one (Gonzalez & Wintz 1987). Sometimes the same techniques can transform hyperspectral space into lower dimensional space like *principal component* and *canonical variate* analyses (Schmidt 2003). Another valuable technique is the Minimum Noise Fraction (MNF) transformation, which as Van Der Meer and De Jong (2003) explain, uses a two-step principal, in which components transform to first decorrelate noise in the image to have unit variance and then ranks components in terms of decreasing signal to noise ratio (SNR). This technique has the effect of reducing the dimensionality of the image data, which in turn reduces the storage, computational power and time required to process the data. Importantly, it also allows data with a relatively high SNR to be identified and retained for analysis. In addition, the continuum removal algorithm was used to transform reference spectra and image data to enhance the comparison of individual absorption features prior to classification and to serve as input to the Spectral Feature Fitting (SFF) algorithm.

Sub-pixel analysis targets features smaller than the pixel size. Depending on the level of spectral contrast, very small quantities can also be estimated using mixture modelling. Complete *linear spectral unmixing* demands all the surface materials and their pure signatures to be known (Boardman 1989). Ahn, Baumgardner and Biehl (1999) analysed AVIRIS images for soil mapping by using *linear mixture modelling* where all soil patterns were known. This may not be the case in many instances. An alternative to 'complete' mixture modelling approach is *mixture-tuned matched filtering* (MTMF) which offers a pragmatic solution in the form of partial unmixing (Dehaan & Taylor 2003).

In order to achieve a defined objective while using hyperspectral images, one may resort to more than one technique especially at the exploratory stage. In this study, both whole pixel (Maximum Likelihood, Spectral Angle Mapper, Spectral Feature Fitting) and sub-pixel (MTMF) techniques have been tested separately and in combination.

2 Background

Despite considerable expenditure of public and private funds (the Victorian Auditor General estimated $1.8 billion over the period 1990-2001) the Victorian Government still does not have a reliable measure of the outcome of the salinity management program that can be used to report at landscape scale. This is limiting the ability to implement and measure the effectiveness of key Commonwealth and State Government policies. Land salinity has been accepted as one of the Matters for Target indicators within the *National Framework for Natural Resource Management Standards and Targets* and the extent and severity of land salinity been listed by the Victorian Government as one of the Victorian Catchment indicators. The 'Growing Victoria Together' program emphasises the need to protect the environment for future generations, promote sustainable development and improve the health of our rivers and waterways by taking action to reduce salinity. It aims to produce a measurable reduction in the environmental and economic impact of salinity by 2015. In addition, the Commissioner for Environmental Sustainability has a statutory requirement to encourage ecologically sustainable development (ESD), report on the state of environment in Victoria and advise the Minister for Environment on matters relating to ESD.

Current field based methods commonly used to map and monitor land salinity are considered to be too expensive and labour intensive to implement at a statewide level. Airborne and satellite based multi-spectral sensors have been advocated as technologies for reducing the cost of field based measurement of soil salinity. But, multi-spectral sensors are limited spectrally usually with less than 10 relatively broad bands (typically in the range 50 to 100 nm). Rather than identifying saline soil or salt-tolerant vegetation, multi-spectral sensors rely on surrogate measurements e.g. the National Action Plan (NAP) recently funded a trial in the Wimmera of techniques developed by CSIRO (Furby & Clark 2003). The project used multi-spectral sensors (e.g. Landsat MSS, TM and ETM+) to map areas of consistently poor growth as a surrogate for soil salinity. This approach works well in some environments, but is likely to be limited in moderately and slightly saline areas where salt-tolerant species can still thrive and maintain good ground cover. In contrast, hyperspectral sensors with over 100 narrow spectral bands (typically < 20 nm) have a much greater ability to differentiate vegetation down to genera and in some cases species level. These sensors have the potential to significantly reduce the cost of mapping and monitoring the extent and severity of soil salinity based on the presence of salt-tolerant species while maintaining the accuracy of the current field based method.

Victoria led the national dryland salinity effort in the late 1980s and early 1990s, and salinity management plans framed at that time set the direction for onground works and research aimed at combating salinity. The plans used cost-benefit analyses based on assumptions of what was likely to happen if the salinity was not addressed. There has been little reassessment of the effectiveness of the works carried out to date, or how the extent of salinity has changed since the plans commenced operation. Without reliable monitoring data, appropriate management decisions cannot be made or funds targeted to the best advantage of the whole community.

Accurate timely data showing changes in soil salinity will provide valuable input to 'triple bottom line' performance indicators used in Victorian and Commonwealth State of the Environment reporting, Victorian Catchment Management Council (VCMC) and Catchment Management Authority (CMA) based reporting on condition and trends. It will also allow CMAs to identify priority areas for action, set meaningful targets and monitor performance against targets within the priority areas.

This study is aimed at identifying saline soils based primarily on the presence of salt-tolerant vegetation and the absence of salt-sensitive vegetation rather than identifying saline soils directly. The effect of salt on the mineralogy of soil and the ability to identify and map such soil is examined only briefly and is, to a large extent, outside the scope of this project. In this study, reflectance of the soil component is only examined to identify any correlation between salt content and surface reflectance, and to account for the contribution that the soil component makes to the average reflectance for a given pixel.

The reason for this approach is that a significant amount of Victoria's salinity occurs where climate, soil, geology, hydrogeological processes and land use combine to produce salt affected areas characterised by a consistently good cover of salt-tolerant vegetation, a reduction in, or absence of, salt-sensitive vegetation and few areas of bare soil. Salt scald or surface salt crust is rarely present. The vegetation in and around these sites is often composed of grasses and herbs. At sites like these, the level of soil salinity is not extreme and they may be termed mesohaline, meaning medium levels of soil salinity. Soil salinity of this type frequently is a result of change in land use and management following European settlement and is known as secondary salinity. Sites of this nature differ with those common in Victoria's north west where relatively low rainfall (less than 400 mm per annum) and high rates of evaporation combine with hydrogeology, geology and soil type to produce areas of very high soil salinity. Saline sites in this region are typically characterised by large amounts of bare soil, often showing surficial salt scald or crusting and the vegetation is primarily salt-tolerant indigenous perennial vegetation. Such sites often existed prior to European settlement and are known as primary sites. This type of environment may be termed euhaline, meaning extremely saline. In remote sensing terms, the level of contrast with surrounding non-saline areas at euhaline sites is relatively high compared to the contrast seen at mesohaline sites. If we are to develop a tool for monitoring soil salinity it is important that it is effective and reliable across all of the major saline environments common in Victoria.

3 Study area

This study was conducted in Victoria's Western District approximately 10 km north of Hamilton (see Figure 1). The climate is mild and the average annual rainfall is around 700 mm. The bulk of the annual rain falls between April and November with the period January to March being the driest time, although paradoxically the heaviest falls tend to occur between December and April. Evaporation in this region is relatively low when considered in a statewide context, but it is probably safe to assume that taken over a whole year, it will exceed annual rainfall, although direct measurements of evaporation are scarce. However, there is potential for recharge all year round depending on the soil moisture levels. The growing season at Hamilton is around seven months starting in April, but low temperatures through the middle of winter may reduce plant production dramatically. The main farming enterprise is grazing to produce wool, although prime lambs, beef cattle and agroforestry are becoming more prominent. The site is located on a broad undulating basalt plain formed during the Pliocene epoch of the Tertiary period sometime in the last 2 million years (LCC 1978).

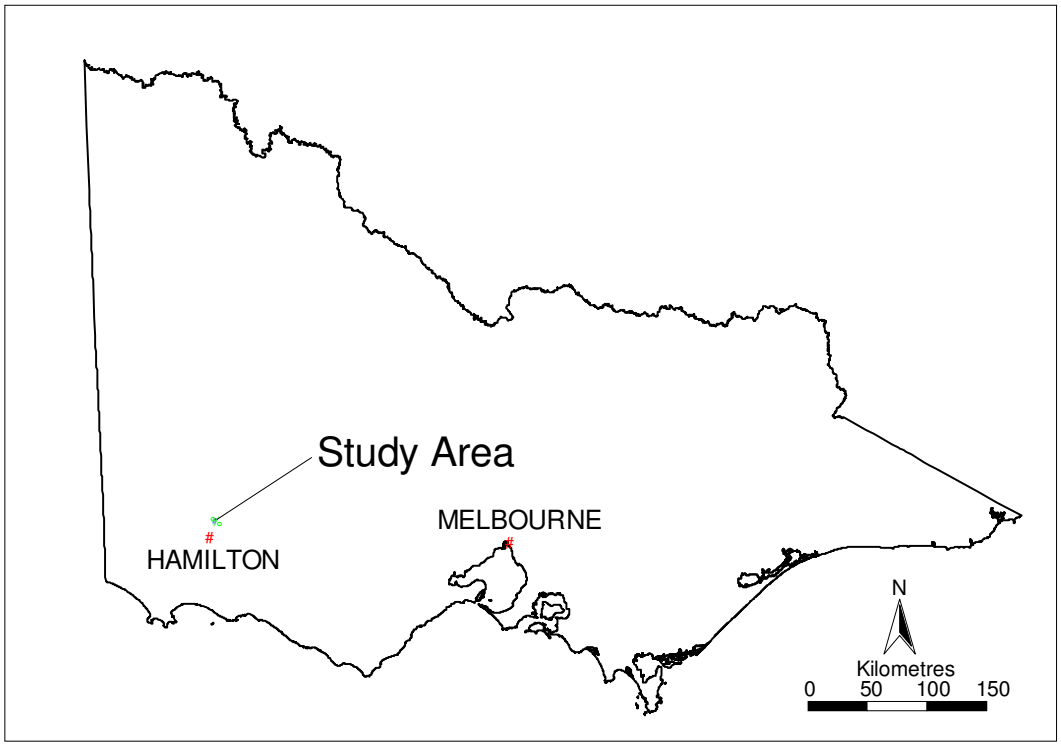

Figure 1 Location diagram for the study area

The level of soil salinity in the study area is mostly in the low to high range (EC_e 2-16 dS/m) and is generally located in drainage lines associated with the edge of basalt flows (Bennetts, Webb & Gray 2003). In this mesohaline environment, the salt affected areas tend to be characterised by a good cover of salt-tolerant vegetation, the absence of salt-sensitive vegetation and little bare soil. Due to a combination of relatively high rainfall, low evaporation, geology and soils, the extreme conditions found in euhaline environments are not common in this region.

4 Method

4.1 Hyperspectral image data

The hyperspectral image data was collected by HyVista Corporation using the airborne HyMap sensor. The HyMap sensor is an optomechanically scanned system incorporating spectographic/detector array modules, on-board reference lamp and a shutter synchronised to scan line readouts for dark current monitoring. The fully enclosed system is mounted in a three axis, gyro-stabilised platform (Cocks et al. 1998). The spectral configuration for the sensor is shown in Table 1.

Table 1 Spectral configuration for the HyMap airborne sensor.

Sensor module	Spectral range nm	Bandwidth across module nm	Average spectral sampling interval nm
Visible (VIS)	450-890	15–16	15
Near infrared (NIR)	890–1350	15–16	15
Short wave infrared 1 (SWIR1)	1400–1800	15–16	13
Short wave infrared 2 (SWIR2)	1950-2480	18–20	17

For this project, 12 swathes were collected on the 16th December 2004 with 125 spectral bands and 3 m ground resolution. Each swathe was 1500 m wide. Swathes 1, 2 and 3 were adjacent to each other in a group 10 km north of Hamilton near the airport. Swathes 4, 5 and 6 formed a second group at Warrayure, located 20 km east of Hamilton. Swathes 7, 8 and 9 formed a third group 10 km south of Hamilton at the Department of Primary Industries Pastoral and Veterinary Institute. Swathes 10, 11 and 12 were isolated from each other, but all were 10 to 20 km south of Hamilton.

Appendix 1 shows the sun azimuth at the time of image acquisition (US Naval Observatory 2006) and the sensor heading.

4.2 Field and laboratory data

Collecting vegetation training areas and validation data
Due to the short project timeframe, training and validation data were collected simultaneously. All field data was located using a differentially corrected Global Positioning System (GPS) instrument capable of achieving a spatial accuracy of +/- 2 m.

Training sites consisting of relatively homogenous areas of salt-tolerant vegetation species were identified and mapped in the field using a GPS instrument. A number of salt-tolerant species exist in the study area, but training areas were only mapped in the field for the major salt-tolerant species i.e. those species which cover a significant proportion of the salt affected areas in the image swathe. In practice, it is uncommon to find large stands of one pure species, and the training areas usually consist of vegetation communities composed of a several species common to the salt affected areas. Dehaan and Taylor (2002) use the term 'terrain elements' to describe homogenous areas of soil and vegetation cover that have distinctive spectral properties at the scale measured by the hyperspectral sensor. As it is composed of a mixture of vegetation and soil, a terrain element is not an endmember in the classic sense but may be viewed as providing reference spectra for a terrain element common in the image. It is likely that only the major species in a

terrain element will have a significant influence on the reflectance measured by the hyperspectral sensor, although other relatively minor species (in terms of area covered) may influence the reflectance signal to some degree. To account for this potential variation, additional reference sites were mapped for each major salt-tolerant species where the minor component of the terrain element was considered to vary significantly from other reference sites. The training sites were as large as possible while maintaining a high degree of homogeneity and selected so that the boundaries of the training sites were generally well away from any vegetation boundaries. Given the image spatial resolution and the GPS accuracy, a rule of thumb was that training sites should not be less than 10m x 10m.

Training sites for major salt-sensitive species and other significant land cover classes were identified using landholder knowledge and land cover type at the time of image acquisition was documented for a number of paddocks across the dpi02 image swathe. As they generally cover much larger areas than the salt-tolerant vegetation, or are easily identified, training sites for salt-sensitive vegetation and other significant classes such as water and built infrastructure were generally able to be reliably identified on the image with landholder assistance and were not mapped in the field.

All training data was used to identify pixels in the imagery that corresponded with areas dominated by salt-tolerant and salt-sensitive vegetation and other significant land cover classes. These pixels were used to train the classification algorithm to find other sites with similar spectral characteristics within the image.

In order to assess the accuracy of the image analysis, validation data was collected in the field to compare against the image classification. To ensure a statistically rigorous accuracy assessment, the minimum number of validation sites needed to determine sensitivity (proportion of saline sites correctly identified by image classification) and specificity (proportion of non-saline sites correctly identified by image classification) to +/- 5 and 10% (90% confidence limits) was determined by applying binomial distribution theory and is shown in Table 2. None of the validation sites were used as training data. The site for each validation point was determined using a stratified random process that was applied to previous soil salinity ground-based surveys held in the DPI/DSE Corporate Geospatial Data Library (CGDL) i.e. validation points were randomly selected from previously mapped salt affected areas and known non-saline areas within the image swathe. For the saline class, 111 points were located and verified in the field. For the non-saline class, 155 points were located and verified in the field. This easily satisfied the number of sites specified in Table 2.

Table 2 The number of validation sites needed to determine sensitivity (proportion of saline sites correctly identified by image classification) and specificity (proportion of non-saline sites correctly identified by image classification) to +/-5 and 10% (90% confidence limits).

Sensitivity / specificity	**Number of saline and non-saline validation sites needed**	
%	Confidence limits ± 5%	Confidence limits ± 10%
65	246	62
75	203	51
85	138	34
95	51	13

Each nominated point was located in the field using a GPS and its salinity status confirmed or amended based on the standard vegetation based field assessment (Allan 1996). To assist the analysis process, a short description of the dominant vegetation species present, percentage cover for each species, amount of bare soil and the extent of the area to which the assessment could applied, was recorded for each validation site. Notes were also made if a distinct vegetation boundary was nearby and photographs were taken at some sites.

Laboratory measured vegetation spectra

The week following the HyMap image acquisition, vegetation samples were collected for 15 species common to the study area that were known to be either salt-tolerant or salt-sensitive (see Table 3). Spectral

measurements were made under controlled illumination conditions in a laboratory and the reference spectra used as input for the classification algorithms.

Table 3 Plant species collected for spectral measurement.

Common name	Botanical name	Salt tolerance
Sea barley grass	*Critesion marinum*	salt-tolerant
Spiny rush	*Juncus acutus*	salt-tolerant
Tall wheat grass	*Lophopyrum elongatum*	salt-tolerant
Bucks horn plantain	*Plantago coronopus*	salt-tolerant
Danthonia	*Austrodanthonia* sp.	salt-sensitive
Stipa sp.	*Austrostipa* sp.	salt-sensitive
Kangaroo grass	*Themeda triandra*	salt-sensitive
Sweet vernal grass	*Antoxanthum odoratum*	salt-sensitive
Cocksfoot	*Dactylis glomerata*	salt-sensitive
Yorkshire fog grass	*Holcus lanatus*	salt-sensitive
Barley grass	*Hordeum leporinum*	salt-sensitive
Perennial rye grass	*Lolium perenne*	salt-sensitive
Phalaris	*Phalaris aquaticus*	salt-sensitive
Broad leaf plantain	*Plantago lanceolata*	salt-sensitive
Sub clover	*Trifolium subterraneum*	salt-sensitive

Collection and preparation of vegetation samples

For each of the 15 species, 20 samples were collected. When plants were collected in the field they were cut as low to the ground as possible and then cut into 15-20 cm lengths if required. The basal section was placed in the bag first, with the next section placed on top of it. This continued until the uppermost section of the plant (generally containing the flower or seed heads) was placed on top of the plant material. After cutting, each sample was packed in a labelled plastic bag and stored in a refrigerator for transport back to the laboratory. All plants were kept refrigerated until their spectrum was measured. Spectra were measured for all samples within three hours of cutting to minimise deterioration of the plant material (Matthews, Clark & Callinan 2006).

Laboratory measurement of vegetation spectra (vegetation reference spectra)

For each sample, five spectral measurements were made. Laboratory measurement of spectra was carried out in an environment where the amount and type of illumination could be controlled. To this end, a box was positioned over the spectrometer and the vegetation sample to exclude natural light. The inside of the box and all fittings inside the box were painted matt black to reduce reflectance from background materials on the spectrometer sensor. A pair of 50 W quartz-tungsten halogen lights were installed inside the box 70 cm either side of, and 90 cm above, the sample. The lights were powered by a 12 volt DC source to ensure a constant current. The spectrometer has a conical field of view (FOV) of 25 degrees and was located so that the sensor aperture was 30 cm directly above the plate on which the vegetation samples were placed. At this height the diameter of the FOV was just over 13 cm. The plate was covered by a matt black material that contributed very little to the reflectance measurement.

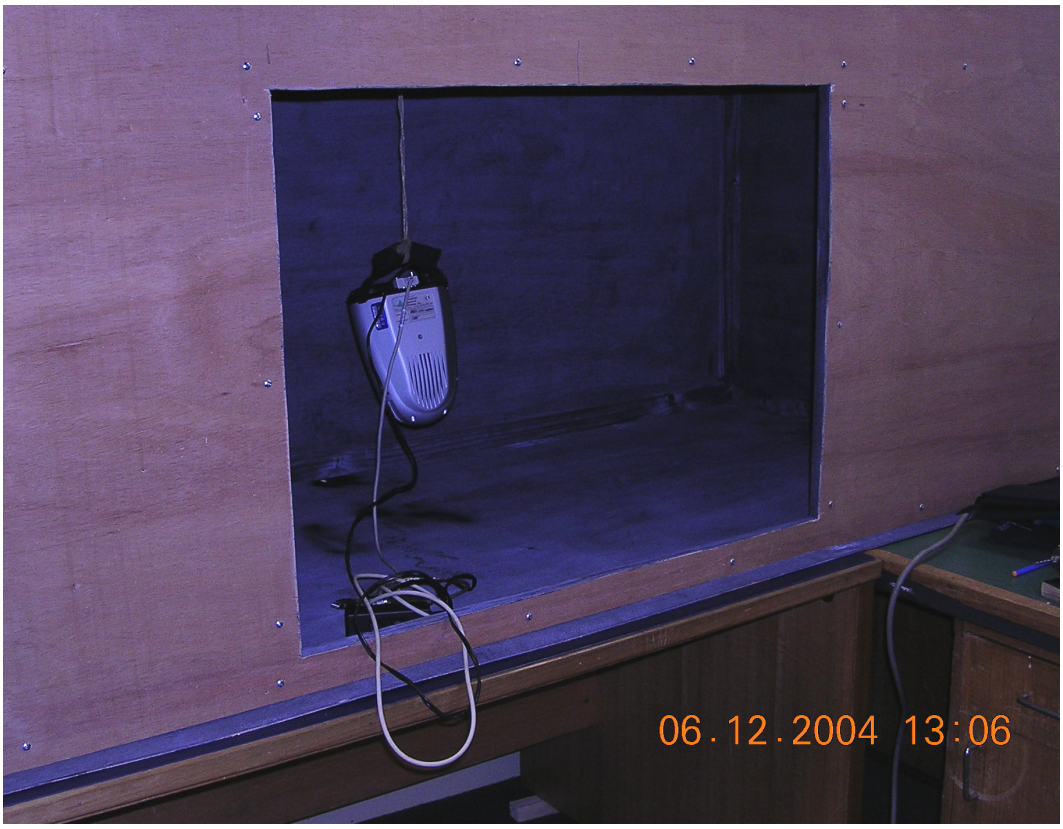

Figure 2 The VNIR spectrometer set up in a darkened box to control illumination for measuring vegetation spectra

The instrument used to measure the vegetation spectra was an ASD FieldSpec HandHeld VNIR spectrometer. Table 4 lists the instrument specifications (Matthews, Clark & Callinan. 2006).

Table 4 Technical specifications for the ASD Fieldspec Handheld VNIR spectrometer.

Number of bands	512
Spectral range	325-1075 nm
Band width	1.6 nm
Spectral resolution	3.5 nm at 700 nm
Field of view	25 degrees

Collecting soil samples in the field

Soils were sampled and analysed to develop an understanding of their contribution to reflectance data and to evaluate the ability to predict the difference between saline and non-saline exposed soils based on their reflectance spectra. Soil samples were collected from saline and non-saline areas identified using previous field-based soil salinity surveys held on the CGDL soilsal25 layer and areas of exposed soil identified on the HyMap images.

The number and spatial distribution of soil sample sites was primarily determined by the salinity rating according to previous field salinity assessment held on the CGDL. Factors such as the intensity of grazing, position in the landscape, vegetation type and degree of cover also influenced the choice and number of sites. Saline discharge areas were assessed by initial field inspection with four to six sites chosen for

sampling areas. Bare earth sites that were non-saline were also sampled to enable a comparison of saline and non-saline soil spectra and soil parameters.

Numerous studies (Chabrillat et al. 2002; Leone & Sommer 2000; Wu et al. 2005) have used different methods for collecting soils spectra including field and laboratory analysis. For this project, soils were collected from field locations and then analysed in the laboratory to ascertain chemical, physical and spectral properties. Soils collected for laboratory analysis of spectral properties are often disturbed samples that have been dried, sieved and mixed as homogenous samples. However, this often does not replicate soil properties in the field and the resultant reflectance soil spectra. With this in mind, soil samples were collected in various forms to replicate properties of soil in the field and impacts of drying and sieving. Disturbed samples were scraped from the surface soil (top 1-2 cm) using a spatula. Undisturbed samples were collected as intact soil cores about 70 mm in diameter and 70 mm in depth (See Appendix 2 for the soil sampling procedure). The undisturbed samples were collected with the principal aim of preserving the original soil surface. This was potentially important due to the soils exhibiting possible surface crusting characteristics owing to concentrations of evaporite minerals.

Laboratory measurement of soil spectra (soil reference spectra)

Absorption features related to iron content in soils occur at wavelengths below 1000 nm in the VNIR region of the spectrum, but the main absorption features used to identify clay mineralogy occur in the short wave infrared (SWIR) region of the spectrum between 2000 nm and 2500 nm (Van Der Meer & De Jong 2003). To account for the wavelengths of the significant absorption features, spectral measurements for soil samples were made using an ASD FieldSpec Pro FR spectroradiometer. This instrument uses three detectors to cover the spectral range 350-2500 nm. The technical specifications for the instrument are listed in Table 5. This spectrometer has a conical field of view (FOV) of eight degrees and was located so that the sensor aperture was 20 cm directly above the plate on which the soil samples were placed. At this height the diameter of the FOV was just under 3 cm across each soil sample.

For each soil sample, five spectral measurements were made. Laboratory measurement of soil spectra was carried out in a similar environment and using the same illumination system as for the vegetation samples.

Table 5 Technical specifications for the ASD FieldSpec Pro FR spectrometer.

Detector	**Visible Near InfraRed (VNIR)**	**Short Wave InfraRed 1 (SWIR1)**	**Short Wave InfraRed 2 (SWIR2)**
Spectral range (nm)	350-1050	900–1850	1700-2500
Band width (nm)	1.4	~2	~2
Spectral resolution (nm)	~3 (at 700 nm)	10–12	10–12
Field of view (degrees)	8	8	8

Soil analyses
Owing to the collection of disturbed and undisturbed soil surface samples, samples were analysed under set conditions to replicate different soil states including moisture content, surface integrity and particle size. The combination of soil states included:

- undisturbed and of field moisture
- undisturbed and oven dried
- disturbed and oven dried
- disturbed, oven dried and sieved.

The field moisture content for samples was determined by first weighing the soils at field moisture. Samples were then oven dried at 105°C for 48 hours, weighed, then dried at 105°C for another 24 hours before reweighing to confirm soils are dry. A subset of disturbed soil samples were sieved (2 mm) after drying.

During collection of samples, a number of field tests were undertaken including field pH using the Inoculo soil pH test kit, field texture grade (McDonald et al. 1990), effervescence of carbonate in fine earth (McDonald et al. 1990) and soil colour.

A suite of 18 samples was analysed for wet chemistry including pH (H_2O and $CaCl_2$), electrical conductivity (1:5), total soluble salts and soluble chloride. These tests were analysed to determine the concentrations of salt in each sample to characterise saline and non-saline soils. From the 18 samples, a subset of 10 were analysed for their X-ray diffraction patterns to identify the constituent minerals for each sample. The soil salinity levels of each sample were examined in conjunction with its mineralogy to identify if indicator minerals existed for saline and non-saline soils, therefore allowing better prediction of salinity levels of exposed soils using spectral libraries of these minerals and the HyMap spectral data. The procedure along with mineralogical composition of samples is provided in Appendix 3.

4.3 Image processing

Some processing of the image data was required prior to analysis to remove systematic and random error caused by atmospheric effects and distortion, degradation and noise introduced in the imaging process (Jensen 1996). Image data is also transformed to assist in the analysis and as input for some of the classification algorithms.

Atmospheric correction
HyVista Corporation supplies both radiance calibrated (at sensor) data and atmospherically corrected (apparent reflectance) data. HyVista apply the HyCorr algorithm to correct the effect of the atmosphere on radiance data, and EFFORT polishing (Empirical Flat Field Optimal Reflectance Transformation) to remove consistent noise or error features that may appear in apparent reflectance data.

Initial inspection of the HyVista reflectance data suggested that the data lacked detail and to some extent it appeared to be over-smoothed. To check this, the HyVista radiance data was corrected for atmospheric effects using ACORN 4.0 (Atmospheric CORrection Now) software to produce radiance data without additional smoothing by the EFFORT algorithm. Both datasets were compared across a range of ground cover types and no significant differences were found. This study used the HyMap apparent reflectance data produced using the HyCorr algorithm with EFFORT polishing for all image processing.

Cross image brightness gradients
Image analysis can be affected adversely by cross image brightness gradients. Size of the field of view (FOV) and direction of the sensor at time of acquisition relative to the sun are important factors. Cross track brightness gradient effects are greatest at the edge of the images and when the flight path is perpendicular

to the sun-target-observer plane. The effect is reduced when the flight path is in line with the sun-target-observer plane and is usually insignificant at the nadir (Schiefer, Hostert & Damm. 2006).A number of the image swathes supplied by HyVista appeared to contain cross image brightness gradients. Comparison with data obtained from the US Naval Observatory site (US Naval Observatory 2006) showed the azimuth at the time that the HyMap image was acquired (see Appendix 1). The difference between the sensor heading and sun azimuth for swathes dpi01, dpi02 and dpi03 was less than five degrees. The difference for swathes dpi04, dpi05 and dpi06 ranged from 30 to 40 degrees and for swathes dpi07 to dpi12 ranged from 70 to 80 degrees. This indicated that swathes dpi04 through to dpi12 were likely to have significant cross image brightness gradients and concurred with the visual inspection. Accordingly swathes dpi04 to dpi12 were excluded from the analysis. The three remaining swathes (dpi01, 02 and 03) appeared to have no variation in cross scene reflectance, and accordingly no correction for cross track brightness gradients was applied. These swathes were adjacent to each other and almost all salinity in this area was restricted to dpi02. To meet project milestones within the specified timeframe, all analyses were restricted to swathe dpi02. All image processing and analysis for this project was performed using the ENvironment for Visualising Images (ENVI) version 4.2 software (Research Systems Incorporated, Boulder, Colorado).

Image rectification

Images are geo-rectified so that it is possible to identify training areas on the ground that may not stand out in the image, but are known to contain unique and homogeneous ground cover types that will be useful for training classification algorithms. As well, georectification allows post-classification comparison with independent validation data. There are arguments within the remote sensing community about errors that may be introduced by the resampling of data that occurs in the geo-rectification procedure. In this project reference spectra were collected from rectified images to take advantage of training areas identified on the ground using GPS instruments. However, to minimise the effect of any resampling error on the classifications, all classifications used non-rectified images. Classified images were then georectified post classification to allow comparison with ground validation points.

The image was geo-rectified in a two stage process. The first stage used the Geographic Lookup Table (.glt) file provided by HyVista Corporation with the image data, and the second stage warped the geometry corrected file using ground control points (GCPs) collected in the field with a differentially corrected GPS instrument. The image was warped using a second degree polynomial and resampled using the nearest neighbour algorithm. Using this process, the dpi02 swathe was geo-rectified with a Root Mean Square (RMS) error of 0.84 pixels (equivalent to 2.52 m).

Data transformation

Several data transformation techniques were applied to accommodate various classification algorithms and to improve classification results.

The un-rectified image was transformed using the Minimum Noise Fraction (MNF) algorithm both to reduce the dimensionality of the data and to improve the signal to noise ratio (SNR) by separating noise from the data to improve image analysis. MNF transformed data is required for the Mixture Tuned Matched Filtering (MTMF) algorithm and for identifying spectral endmembers within the image. It was also used as an alternative input for the spectral angle mapper (SAM) algorithm and the maximum likelihood supervised classification. Visual inspection of the MNF transformed data and the eigenvalues calculated for each band showed that only MNF bands 1 to 25 were usable. Bands 26 to 125 were assessed as having a poor SNR ratio. All operations using MNF transformed data was restricted to these bands.

Reference spectra libraries and image data were also transformed using the continuum removal algorithm to enhance the comparison of individual absorption features prior to classification and to serve as input to the Spectral Feature Fitting (SFF) algorithm. The continuum removal algorithm normalises reflectance spectra to allow comparison of individual absorption features from a common baseline. The continuum is a convex hull fit over the top of a spectrum using straight-line segments that connect local spectra maxima. The continuum is removed by dividing it into the spectral reflectance value for each pixel (Research Systems Incorporated 2000).

4.4 Spectral processing

Identifying image reference spectra
Prior to classification, the geo-rectified image was examined to determine if known ground features had unique spectra. To this end, spectra were collected from the georectified image using training areas mapped with GPS during the ground survey and using land cover maps provided by landholders. Both reflectance and continuum removed spectral libraries were produced. These spectral libraries were used as reference spectra to characterise the land cover mixtures typical within the image and formed a significant part of the input for several of the classification algorithms.

Identifying image endmembers
As well as reference spectra, the most spectrally extreme pixels (known as endmembers) were identified using the MNF transformed data from an unrectified image via the Pixel Purity Index (PPI) algorithm. A threshold of two was set to ensure that the endmembers identified were relatively pure rather than mixed. To make identification of endmembers easier, the number of pure pixels was restricted to around 2000 by adjusting the threshold for the number of times each pixel was identified. These pixels were projected and rotated in n-dimensional space and groups of pixels that stayed coherent and unique throughout the rotation were identified as endmember classes. By comparison of the unrectified image with the georectified image the 'real world' character of the endmember pixels was identified and noted.

4.5 Image analysis

Whole pixel classification
Whole pixel classification techniques (maximum likelihood supervised classification and the SAM algorithm) were applied both to reflectance data and MNF transformed data, while the Spectral Feature Fitting (SFF) algorithm was applied to continuum removed data.

Maximum Likelihood Supervised Classification algorithm
The maximum likelihood classification was run on un-rectified image data in two ways:

- Reflectance image and image reference spectra
- MNF transformed reflectance image and image reference spectra.

Maximum likelihood classified images were geo-rectified using the two stage process described in section 4.3.3 after classification to allow validation against the ground truth data.

SAM algorithm
The SAM algorithm was run on combinations of various un-rectified image data, reference spectra and classification parameters:

- Reflectance image with endmembers generated using the PPI algorithm, with the SAM threshold set to 0.1 radians
- Reflectance image with image reference spectra, with the SAM threshold set to 0.1 radians
- Reflectance image with image reference spectra, with no SAM threshold set
- Reflectance image with vegetation reference spectra, with no SAM threshold set
- MNF transformed data using image reference spectra, with no SAM threshold set.

SAM classified images were geo-rectified using the two stage process described in section 4.3.3 after classification to allow validation against the ground truth data.

SFF algorithm
The SFF algorithm compares the fit of image spectra to selected reference spectra using a least squares technique. Best results are generally achieved when the SFF is run on a single absorption feature. The

reference spectra are scaled to match the image spectra after continuum removal from both datasets (RSI 2000). To this end, the continuum removed versions of the spectral reference libraries were examined and the dominant absorption features for the target land covers identified. They were: 530-730 nm, 910–1040 nm, 1110–1270 nm, 1270–1700 nm, 1700–2250 nm and 2250–2400 nm

The SFF was run independently on each of these absorption features using:

- Image reference spectra
- Vegetation reference spectra

SFF classified images were geo-rectified using the two stage process described in section 4.3.3 after classification.

Sub-pixel classification

A sub-pixel classification using the MTMF algorithm was applied to the data. This algorithm requires that image data and reference data are MNF transformed but does not require knowledge of all endmembers or reference spectra within an image. It also has the ability to detect false positives, thereby improving the analysis results over other sub-pixel classifiers.

The MTMF classification was run on the un-rectified, MNF transformed image using:

- MNF transformed image reference spectra and soil reference spectra. To combine the soil reference spectra with the image reference spectra, the soil reference spectra were resampled and MNF transformed. Both wet and dry soil spectra were included. Appendix 4 presents the complete results of analyses for all soil samples.
- MNF transformed vegetation reference spectra.
- MNF transformed image endmembers.

The MTMF algorithm outputs two bands for each target. One band is a matched filter (MF) score with a range of 0 to 1. The MF score indicates the closeness of fit to the reference spectra for that target and its approximate sub-pixel abundance. A score of 1.0 is a perfect fit. The second band is in units of noise sigma and indicates the feasibility of the MF result. The lower the infeasibility score the more likely that the MF score is a true result and not a false positive. Correctly mapped pixels will have a MF score above the background distribution around zero and a low infeasibility score (RSI 2006). For each target, a ratio of the MF score divided by the infeasibility score was calculated.

To synthesise all the land cover classes and produce a classification of saline and non-saline soil based on the vegetation community rather than the presence of one species, the ratio values for each reference spectra or endmember were run through:

- A maximum likelihood classifier using training areas collected via field surveys and landholder knowledge
- A rule classifier, where the pixel is assigned to the "class" with the highest ratio value for that pixel. If ratio values are equal then the pixel will be assigned to the first class in the list. If a nil threshold is set all pixels will be assigned to a class even if the ratio values are very low.

MTMF classified images were geo-rectified using the 2-stage process described above after classification to allow accuracy assessment using the differentially corrected GPS validation data.

Spatial resampling

To assess the spatial resolution needed to map soil salinity using hypersepctral data, the reflectance data was resampled from the original 3 m pixels to produce images with 15 m and 30 m pixels. The following procedure was applied separately to both 15 m and 30 m images.

The image was MNF transformed and the MTMF algorithm was applied using its own image reference spectra plus soil reference spectra for wet and dry undisturbed samples measured in the laboratory. The image reference spectra were derived for a given spatial resolution by overlaying the training areas mapped in the field and those collected from landholders on the geo-rectified image at that spatial resolution and then only applied to the un-rectified image of that spatial resolution. That is the image

reference spectra for the 15 m pixel image were derived by draping the known training areas over the geo-rectified 15 m image. This reference spectra set was then only applied to the 15 m image. Using the output of the MTMF algorithm, matched filter/infeasibility MTMF ratios were produced for each reference spectra. Each ratio set was then run through a simple rule classifier algorithm to produce a saline or non-saline classification for the trial area.

MTMF classified images were geo-rectified using the two stage process described in section 4.3.3 after classification to allow accuracy assessment using the differentially corrected GPS validation data.

To determine the effect of spatial resolution on the ability to map soil salinity using airborne hyperspectral data the error matrices for the 3 m and the 15 m resolution data and the 3 m and the 30 m resolution data were compared. To this end, the significance of the difference between pairs of error matrices i.e. the 3 m and 15 m resolution and the 3 m and 30 m resolution using the MTMF classifier was determined by the Z statistic for the difference between Kappa (κ) values, since κ is asymptotically normally distributed (Congalton & Green 1998).

Validation

Classification results were validated using the independent test data that was collected in the field (see Section 4.2.1), by comparing each pixel coincident with a ground truth point based on it being either saline or non-saline. Accuracy assessments for each classification are tabulated in Appendix 5 and a summary is tabulated in Table 6 in Section 5.2.

The accuracy of each classification was assessed by comparing the classification results to the reference ground truth data in an error matrix. Congalton and Green (1998) consider that an error matrix provides an effective way of representing classification accuracy as it plainly shows the individual accuracy achieved for each category. The overall accuracy of the classification (the correctly classified samples divided by the total number of sample units) and both the producer's (the probability that all points known to belong to a particular class were correctly identified by a classifier) and user's accuracy (the probability that a pixel classified as being in a particular class will be correct) for saline and non-saline classes is shown. The overall accuracy can be misleading and the producer's and user's accuracy provide a means of identifying if either category was over or under classified by a given algorithm.

5 Results

5.1 Soils

Laboratory spectra for soils
Reflectance spectra for the four soil subsets (undisturbed and of field moisture; undisturbed and oven dried; disturbed and oven dried; and disturbed, oven dried and sieved) were collected over the spectral range of 350 nm to 2500 nm. In reviewing the soil reflectance data, it was apparent that regions of the spectra had considerable noise that would make analysis of data especially difficult. The noise displayed may be due to a low SNR (signal to noise ratio), poor spectral resolution or a combination of both. Regions to display significant noise include 350-450 nm and 1800-2500 nm (see Figure 3). This had significant implications for defining indicator minerals from the spectra as these minerals are often represented in the electromagnetic spectrum as discrete visible inflections at certain wavelengths. Variability in the spectra is further demonstrated by plotting the standard deviation of spectra for each wavelength using the undisturbed oven dried sample set (see Figure 4).

A useful finding of the analysis of wet against dry undisturbed soil was the significant effect of moisture content on soil reflectance, which has been confirmed by others (Bedidi et al. 1992; Bowers & Hanks 1965; Ryan & Lewis n.d.; Stoner & Baumgardner 1980). Dry samples displayed spectral reflectance values 50-150% above that of the wet undisturbed soil samples (Figure 5). Theoretically the prediction of mineral and water absorption features would be vastly improved using the dry samples. However given that the airborne hyperspectral data was derived from soils at field moisture, it is anticipated that best correlations would exist with soil samples approximating field moisture conditions and their collected spectra. Another noteworthy finding was the difference in reflectance data for the disturbed samples that were sieved (2 mm) and unsieved (Figure 6). Here the spectra varies significantly less than the moist/dry undisturbed comparison, however higher reflectance values are derived from the sieved sample set at 700 nm and above. The most likely explanation is that the finer particle size of the sieved sample generates less soil surface roughness , hence less shadowing and higher absorption of radiant light (McCloy 1995).

Soil analyses including XRD
Electrical conductivities for saline soil sites varied between 3.1 and 30.0 dS/m^{-1} with total soluble salts in the range 0.92-8.90 dS/m^{-1}. These values appear high given the visible signs of salinity at the site but are confirmed by the extreme soluble chloride results (see Appendix 4). This may be a result of the sampling method where soils analysed were collected from the soil surface rather than a composite sample from 0 to 10 cm. The XRD patterns of the 10 soil samples identified quartz as the dominant phase, with clays including montmorillonite at minor to trace quantities. Little visible correlation existed between clay mineralogy and halite. As a result, clay mineralogy was not considered to be a useful predictor of salt for this study.

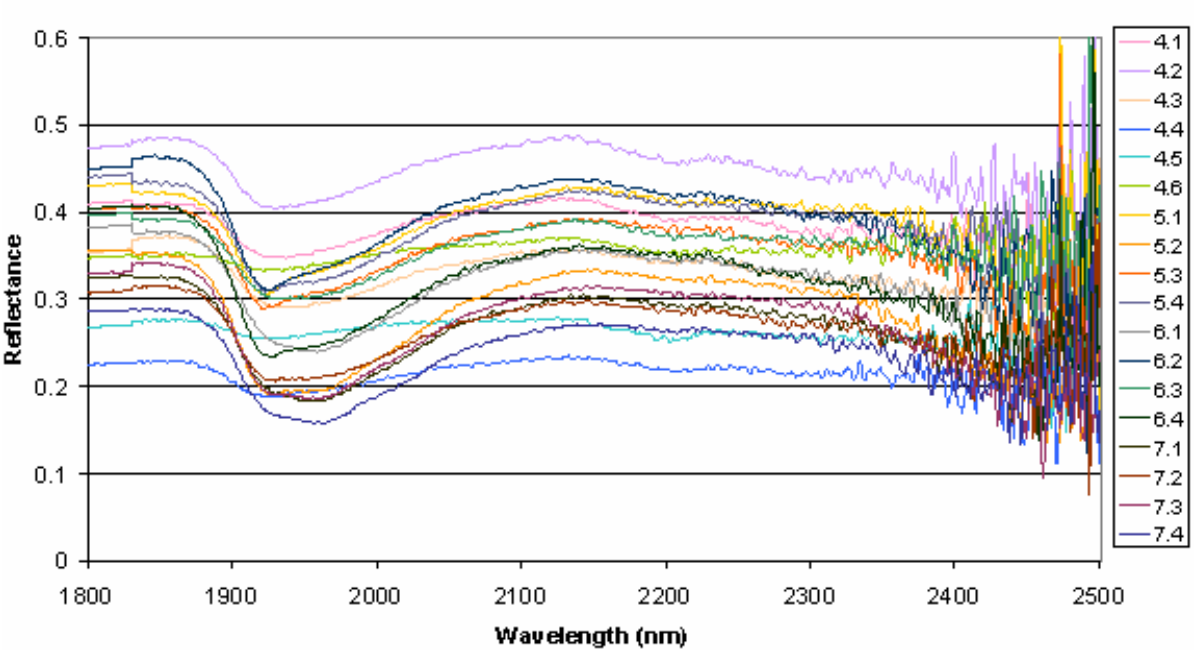

Figure 3 Visible noise in the 1800-2500 nm spectral range for the oven dried undisturbed soil samples (note that all soil subsets display similar noise)

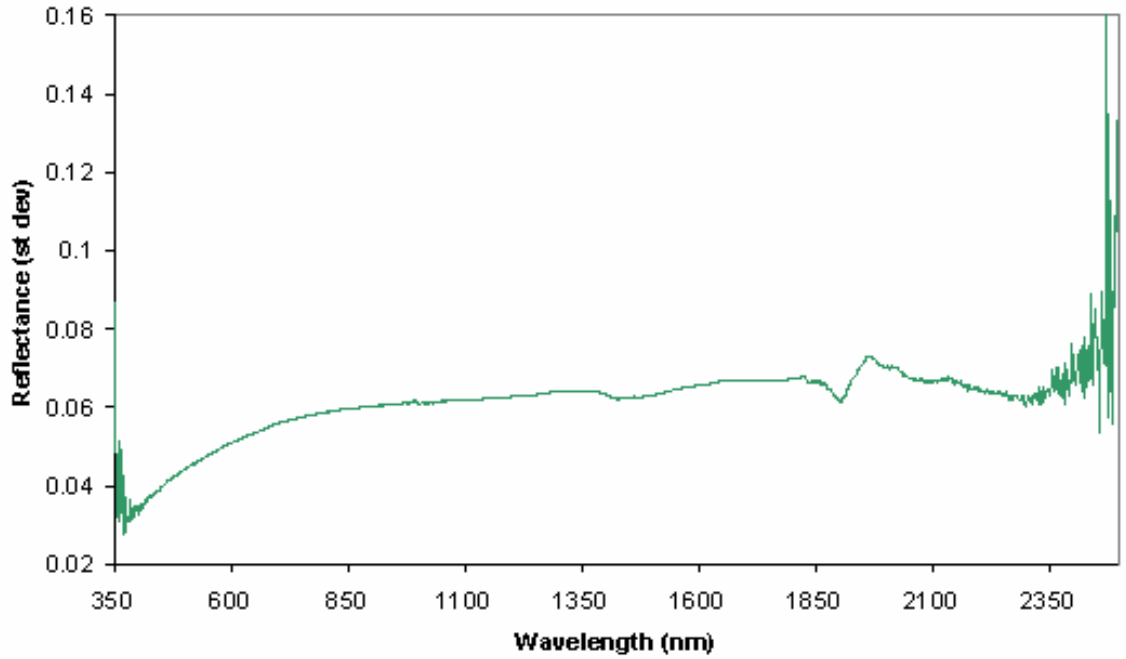

Figure 4 Standard deviation of reflectance data from the oven dried undisturbed soil samples (note that all soil subsets display similar variability)

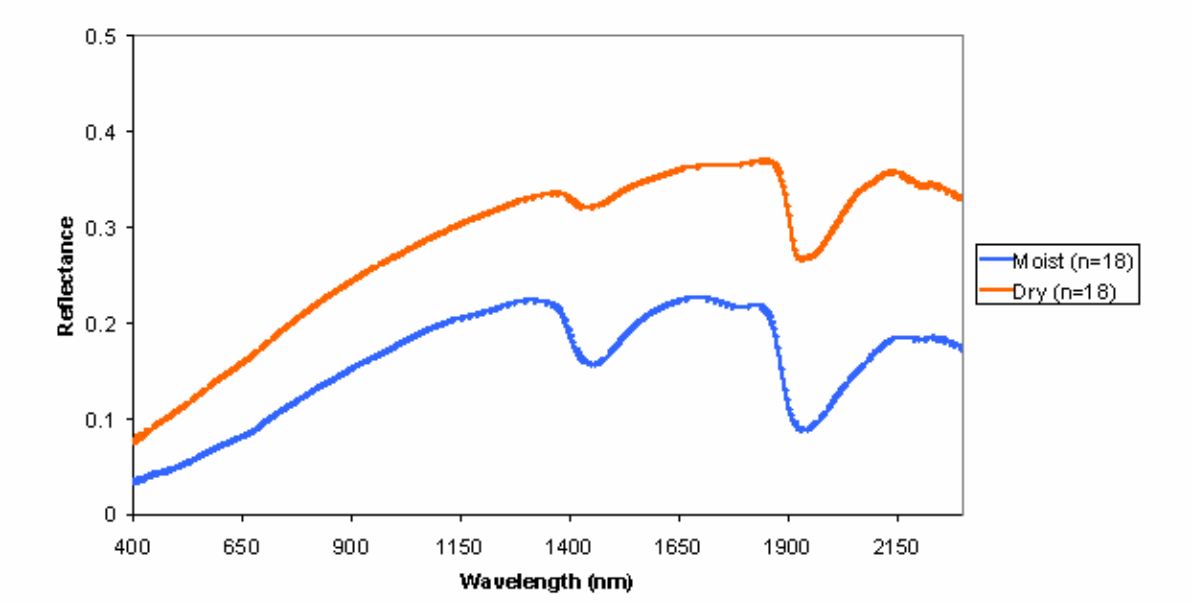

Figure 5 Comparison of spectral reflectance from moist and oven dried undisturbed soil samples

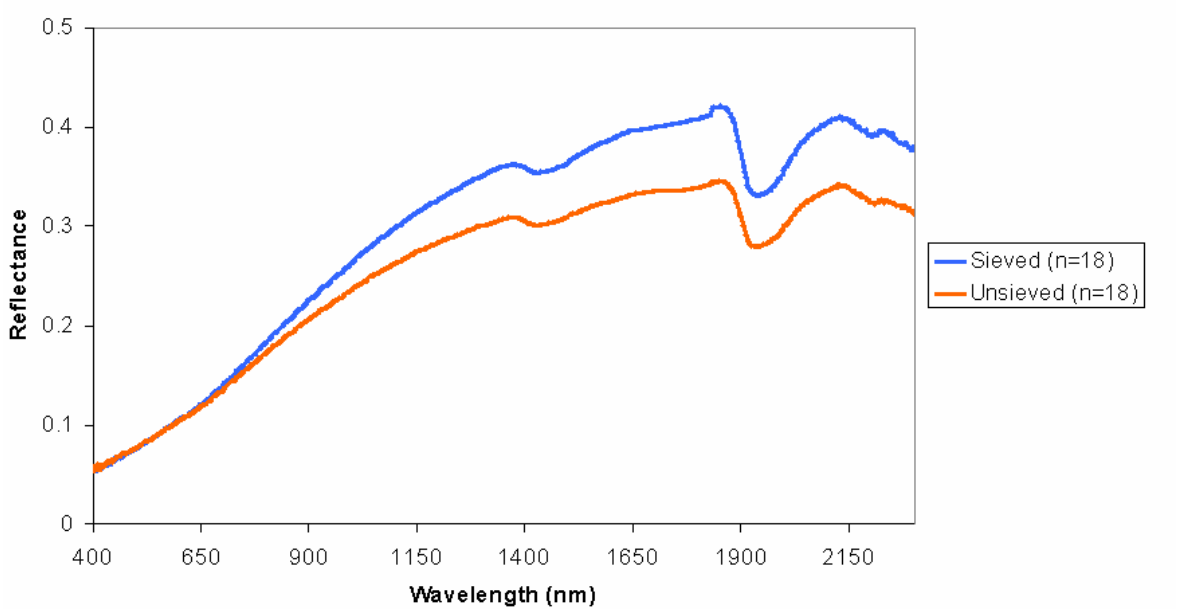

Figure 6 Comparison of reflectance data for the disturbed samples that were sieved (2 mm) and unsieved

5.2 Image analysis

The complete set of results for all image classifications is shown in Appendix 5. Results for the SFF algorithm were not recorded, as initial visual assessment of the results indicated there was little ability to discriminate between reference spectra in the image. As a result, the SFF outputs were not tested against the ground validation data. Results for each classification are displayed in error matrices, where the image classification result for a pixel is compared to the field assessment for the point coincident with that pixel. Each error matrix provides a reliable means of assessing the ability to correctly identify both saline and non-saline soil for each classification algorithm +/- 10% with 90% confidence. From each error matrix the overall accuracy plus the producer's and user's accuracy is calculated.

Table 6 summarises the complete results listed in Appendix 5 and compares the accuracy achieved by the various classification algorithms. It shows that the sub-pixel analysis based on the MTMF algorithm achieved the best results out of all the classifiers. The results achieved by using either the maximum likelihood or the rule classifiers for the second stage of the classification were very similar.

The maximum likelihood classifier performed almost as well as the MTMF based classification when the reflectance image data and the reference spectra were transformed using the MNF algorithm. Its accuracy was affected by a reduced ability to correctly identify land cover classes indicative of both saline and non-saline soil. Both classes (but particularly the non-saline class) were accurately identified with a low error count.

The SAM algorithm performed in a similar fashion to the maximum likelihood classifier when used with the image reference spectra. Its best result was achieved using reflectance spectra, with nil threshold set. This algorithm performed poorly when using the PPI derived endmembers and the vegetation spectra as reference spectra. Both these combinations achieved very poor results for identifying land cover classes associated with saline soil. The reliability of the pixels classified as salt was also poor. The results achieved for both these combinations, for land cover classes associated with non-saline soils was better than for the saline classes, but poorer than that achieved by most other classifier reference spectra combinations.

As previously stated, the best result across all classifiers was achieved using the two-stage classifier based on the MTMF algorithm. This combination achieved the highest overall accuracy and the best result for identifying land cover classes associated with saline soil. The MTMF based classifier using vegetation reference spectra performed relatively poorly, but better than the SAM algorithm with the same reference spectra. This combination did achieve a very high accuracy for non-saline soils when the maximum likelihood classifier was used to look at the community of land cover classes in total. However the vegetation laboratory spectra were not as effective at identifying saline soil as other reference spectra. The MTMF based classifier using PPI derived endmembers achieved a very good overall accuracy, but this was due to an outstanding result for non-saline soils. Its ability to identify land cover associated with saline soil was relatively poor.

The investigation of varying image spatial resolution used the best-performed classifier combination (two-stage classifier with MTMF followed by maximum likelihood) on 15 m and 30 m pixel images that were derived from the original 3 m pixels. Kappa analysis of the confusion matrices showed that there was no significant difference at the 95% confidence level in the ability to differentiate saline soil from non-saline soil when classifying 3 m resolution Hymap image data or 15 m or 30 m resolution data derived from the original Hymap data, when using the two-stage MTMF technique with the image reference spectra augmented by the soil spectra. The Kappa analysis was based on data in Tables 25 to 28 in Appendix 5.

Table 6 Summary of classification accuracy

Classification	Overall accuracy %	Saline soil classification		Non-saline soil classification	
		Producer's accuracy %	User's accuracy %	Producer's accuracy %	User's accuracy %
Maximum likelihood using image ref spectra on reflectance image	73	76	77	71	85
Maximum likelihood using MNF transformed image ref spectra and image	83	78	87	86	96
SAM 1, using PPI endmembers on reflectance image, SAM threshold = 0.1 radians	47	30	62	60	72
SAM 2, using image ref spectra on reflectance image, SAM threshold = 0.1 radians	80	68	82	88	87
SAM 3, using image ref spectra on reflectance image, nil SAM threshold set	85	78	84	89	87
SAM 4, using lab vegetation spectra on reflectance image, nil SAM threshold set	58	35	50	75	63
SAM 5, using MNF transformed image ref spectra and image, nil SAM threshold set	80	81	94	80	94
MTMF 1a, using image ref spectra and lab soil spectra plus maximum likelihood classification	89	85	89	92	91
MTMF 1b, using image ref spectra and lab soil spectra plus rule classifier	89	83	90	94	90
MTMF 2a, using lab vegetation spectra plus maximum likelihood classification	71	40	80	94	68
MTMF 2b, using lab vegetation spectra plus rule classifier	61	55	53	65	68
MTMF 3, using PPI endmembers plus maximum likelihood classification	84	68	93	96	81
MTMF, using field ref spectra and lab soil spectra plus rule classifier on 15 m pixels	86	81	89	90	92
MTMF, using field ref spectra and lab soil spectra plus rule classifier on 30 m pixels	83	73	84	89	88

6 Discussion

The whole pixel classification based on the maximum likelihood algorithm using field spectra performed reasonably well and it appeared that the application of this algorithm to the MNF transformed data was more successful than when it was applied to the HyMap reflectance data. The MNF transformation has the effect of removing background noise within the image thereby improving the SNR in the remaining bands. The MNF transformation has the added advantage that it reduces the dimensionality of the image data, which in turn reduces the storage, computational power and processing time. The maximum likelihood classifier is relatively simple to implement although it is reasonably demanding of computer resources. One disadvantage is that this algorithm is susceptible to variation in illumination both between and within scenes.

The Spectral Angle Mapper (SAM) algorithm is not affected to a great degree by variations in illumination and this presents some advantages when looking to implement landscape scale analysis that requires multiple scenes. It also reduces the effect of cross image brightness gradients. Even for adjacent scenes illumination will vary between scenes and this algorithm offers a means of reducing the effect of this on classification accuracy. Whole pixel classification based on the SAM algorithm had mixed results. SAM classifications based on reference spectra collected in the field applied to either reflectance or MNF transformed data achieved results similar to the maximum likelihood classification using the reference spectra for the MNF transformed data and almost as good as the MTMF sub-pixel classification. However, the SAM classifications using PPI derived endmembers and vegetation spectra measured in the laboratory achieved only poor results. It is likely that the laboratory vegetation spectra gave poor results in part because the SAM classification is a whole pixel classifier. In contrast, the laboratory derived vegetation spectra were each composed entirely of a single vegetation species, and were not in the configuration present in the field due to the sampling procedure. As spectra of a single vegetation species, they are not directly comparable with the typical ground cover which is composed of an intimate mixture of different vegetation species, leaf litter and exposed soil minerals and described by Dehaan and Taylor (2002) as a 'terrain element'. The concept of a terrain element provides an accurate model of the spatial distribution of land cover types as they occur in the field. Each pixel is in effect a terrain element composed of its own unique mix of elements. Using the laboratory spectra as reference spectra for a whole pixel classifier was likely to fail, because pixels composed solely of a single vegetation species minus the effect canopy architecture and with no background soil are extremely rare in practice. The PPI endmembers achieved the worst result with the SAM classifier and this may have been due to the lack of significant difference between the salt-tolerant and salt-sensitive grasses as previously discussed. As well, the extreme and unique endmembers identified as buildings and dam water masked the subtle endmembers that were our particular interest. This may have been improved by masking the dominant endmembers and re-running the PPI algorithm, but this requires further investigation.

It was deemed necessary to further process the MTMF classification as it outputs matched filter and infeasibility scores for individual land cover classes. The matched filter scores indicate the relative abundance of a target material in a given pixel, but it is possible that other material will also be present. Although a salt-tolerant species may be present in a pixel, other salt-sensitive species may be present in sufficient numbers as to indicate that the pixel is non-saline. For this reason it was difficult to use the output from the MTMF algorithm directly to map salt affected soil and it was necessary to find a way to synthesise the sub-pixel abundance for each land cover class to map soil salinity. One of the principles behind identifying soil salinity on the basis of vegetation indicators is that a vegetation community is more reliable than presence of single species. This is because very few plants are obligate halophytes in the sense that they will only grow where soil salinity levels are high. Virtually all the plants found in this mesohaline environment will grow across the broader environment, but raised soil salinity levels appear to offer them a competitive advantage that they lack in other environments. As a result, they tend to be more common in saline areas than in non-saline areas. They are considered to be indicators of soil salinity, but to be more accurate; it is their increased presence in conjunction with reduced numbers of known salt-sensitive species that indicates increasing soil salinity levels. The second stage classifier applied to the MTMF outputs offered the ability to consider the vegetation and soil community as a whole in a pixel rather than

individual land cover classes. There is potential to improve on the accuracy and detail achieved using this sub-pixel approach by undertaking a more detailed analysis of the land cover classes identified on a per pixel basis and application of a more sophisticated second stage classifier. However, budget and time constraints for this project prevented further investigation at this stage.

The MTMF classification based on the PPI generated endmembers performed reasonably well in terms of its overall accuracy, but tended to under-classify the saline areas and over-classify the non-saline areas. The rule classifier was not used as a second stage classifier as the PPI generated endmembers were not clearly linked to known saline features on the ground. The PPI algorithm generally identifies unique spectral features that form a major component of the spectral variance within the whole image. The endmembers identified in this image were dominated by a number of large buildings at the Hamilton Airport and water in some of the dams. Neither of these features formed a significant spatial portion of the image and they were of no interest for our analysis, which was targeted at discriminating salt-tolerant and salt-sensitive grasses and herbs. The inability to target specific endmembers (which may be insignificant in terms of spectral variance for the whole image) is one of the drawbacks of the endmember approach. It may be possible to reduce the effect of the dominant endmembers and identify secondary endmembers that are of specific interest by masking endmembers not of interest e.g. buildings and water that were identified in the first run of the PPI, and re-running the PPI algorithm to identify secondary endmembers [1] (pers. comm.). However, it may be that the targets of interest, in this case salt-tolerant and salt-sensitive grasses and herbs are all very similar within the image spectral space. This is worthy of further investigation, but time and budget constraints of this project prevented more detailed analysis at this stage. One disadvantage of the endmember approach is that it is specific to an image and endmembers are not readily transferable to other images. This may be overcome to some degree by mosaicing images together, prior to identifying endmembers, effectively treating a number of images as one large image. Glenn et al. (2005) suggested that estimating noise statistics from a larger image may improve classification results for discriminating similar vegetation. This approach is not without its problems, as larger images generally require increased computing power, memory and processing time. As well, creating meaningful mosaics from airborne sensors is technically more difficult than mosaicing satellite based imagery.

Reference spectra based on the vegetation spectra collected in the laboratory, generally did not perform well. These spectra were collected the week after the HyMap image was captured and while hot weather at the time would have had some effect on the vegetation, it was considered that the difference would not have been significant. Species for which reference spectra were held were common in the image, but the MTMF classifier was apparently not able to discriminate them well at a sub-pixel level. This may be due in part to the treatment of the vegetation samples prior to the spectral measurement. The sampling procedure effectively destroyed the effect of the canopy architecture i.e. leaf orientation, canopy thickness, shade etc. which results from the growth form that individual species demonstrate. Another factor may have been the difference between the controlled, artificial illumination conditions for the laboratory spectral measurements and the natural illumination present when the HyMap image was captured. The laboratory vegetation measurements indicated that individual species could be discriminated successfully (Matthews, Clark & Callinan 2006), but this difference was more likely to be based solely on pigmentation differences given the method of sample preparation and spectral measurement. However, the poor results achieved using these reference spectra in conjunction with the HyMap image may indicate that laboratory spectra measured in this fashion cannot be directly applied to sub-pixel image analysis. The use of laboratory reference spectra has a number of potential advantages for application of hyperspectral data at landscape scale and spectra from reference libraries has been successfully applied to mineral exploration. However, the application of reference spectra not generated from the input imagery is more difficult when analysis is targeted at vegetation. Vegetation spectra are the product of a number of physiological and physical factors that are often not unique to particular species, but may be found to varying degree in many species. Added to that is the extensive variability that can be found in the spectral response within the foliage of one species in an image (Cochrane 2000) and difference in phenology caused by variation in local environments.

[1] Dr. Remmy Dehaan (lecturer in GIS and Remote Sensing, Charles Sturt University, Wagga Wagga, May 2006)

The Spectral Feature Fitting (SFF) algorithm performed very poorly in this assessment. This is probably due to the similarity in vegetation absorption features. As Price (1992) points out, a relatively small number of factors control the spectral response of vegetation. Vegetation absorption features tend to occupy common wavelengths and depth and shape may be primarily related to a physiological feature such as phenology, leaf/canopy structure or biochemical content rather than species. The SFF algorithm has been used with some success in identifying minerals in exposed landscapes and the absorption features, which characterise various minerals, are often unique in terms of wavelength or shape. In this type of application the inherent properties of the target may be sufficiently unique to create a spectral response that may be identified with some success by this algorithm. Results in this project suggest that the SFF algorithm is probably not suited to discriminating vegetation species of a similar type.

The spatial resolution of the original data was 3 m. Testing showed that it was possible to achieve a similar accuracy using either 15 m or 30 m pixels at the 95% confidence level. This suggests that it would be possible to acquire the airborne data at lower spatial resolution and therefore more cheaply. This may have significant implications in terms of applying this technology at landscape scale. It should be noted that the 15 m and 30 m pixel data was created by combining either 5x5 or 10x10 pixels. The new, larger pixel was assigned the mean value calculated from all the contributing pixels. To achieve a consistent method, reference spectra were derived using either the 15 m or 30 m resampled imagery. This is obviously not the same as collecting data with a sensor with either 15 m or 30 m spatial resolution, but it does give an idea of the possible consequences of collecting data at this resolution.

Airborne data has a number of advantages over data currently captured by satellite-based sensors. Airborne sensors generally have greater spectral and spatial resolution, increased flexibility for timing of data capture and improved SNR ratios. These advantages make it more likely that airborne hyperspectral sensors will be able to discriminate targets that are not possible using current satellite borne sensors. However, there are several disadvantages if airborne data is used at landscape scale. There is a substantial increase in the amount of data required to cover catchment and regional size areas and this will create a number of computational problems. This is outside the scope of this project and will not be considered further in this discussion. However, variation in albedo within and between image swathes is a hurdle that will have to be overcome before airborne imagery can be used for detailed computer-based image analysis at landscape scale. Cross image brightness gradients may cause significant variation in albedo within an image and this was obvious in some of the images supplied by HyVista Corporation for this project. This effect may be reduced considerably by ensuring that the plane is flown either directly toward or away from the sun as data is being acquired. Several algorithms have been developed to deal with this phenomena (RSI 2006; Schiefer, Hostert & Damm 2006) and a detailed discussion is beyond the scope of this report, but suffice to say its effects could be minimized by sound pre-flight planning. Variation in albedo between adjacent swathes is a further complication when trying to use multiple swathes of airborne data at landscape scale. This may be reduced to some extent by ensuring that the plane is always flown either toward or away from the sun, rather than flying one strip toward the sun and then flying the adjacent strip away from the sun. This would increase the cost of data capture and may be prohibitive, depending on the size of the project area. This is a complex problem and cannot be ignored if multiple swathe areas need be processed to achieve the required coverage. An alternative is to treat each strip individually, but this would greatly increase the amount of ground data required and cost of processing. Combining all swathes into a single mosaiced image is preferable and has the potential to achieve higher accuracies (Glenn et al. 2005), but requires that robust techniques are used to ensure a consistent spectral response across swathes prior to mosaicing. Software has been developed to perform these operations and anecdotal reports of its performance are encouraging, but further investigation is recommended before any landscape scale operations are implemented.

This work investigated the potential to identify soil salinity using analysis of hyperspectral data. In the course of the study it became apparent that this type of data and the algorithms developed to analyse and interrogate it provided the capability to extract other information. Hyperspectral data could be applied to other vegetation related tasks such as grassland mapping, weed identification, land cover mapping in agricultural settings, vegetation mapping in forests and monitoring of riparian condition. The technology is

well used by the mining industry for mapping occurrence of mineral outcrops and could also be used for mapping soil types if the level of vegetation cover is not too high (Chabrillat et al. 2002). An examination of related scientific journals demonstrates that these and other applications have been considered, developed and tested. However, relatively few applications have progressed past the trial stage to an operational phase in Australia. Operational applications based on hyperspectral imagery tend to be confined to the mining sector where funding is more plentiful and potential returns relatively high. This technology has considerable potential but there are factors such as cost of data, computational demands, albedo variation between scenes and low SNR, which still impede its uptake at landscape scale. Given the current crop of sensors, it is likely that remote sensing at landscape scale based on hyperspectral data will only move from an experimental phase into an operational phase if multiple outcomes can be achieved with the same dataset i.e. grassland mapping, soil salinity, wetland condition and extent all mapped with the same dataset to an acceptable accuracy. Unless multiple outcomes can be generated from a single dataset, landscape scale analysis based on hyperspectral sensors may have to wait until satellite based sensors achieve satisfactory spatial resolution and SNR values. As field-based methods of monitoring and mapping are becoming less affordable, research in this area should be continued to provide the spur and direction for the development of new sensors. This will allow the natural resource management community to be in a position to optimise the use of these sensors as they come on line.

7 Recommendations

This section sets out a proposed methodology for using hyperspectral data to map soil salinity within individual image swathes and makes suggestions for developing the ability to map across multiple swathes.

The proposed methodology for mapping soil salinity using a single swathe is as follows:

- Acquire images at a time when the salt-tolerant and salt-sensitive vegetation will be shown to best advantage. Typically this is in very late spring or early summer, prior to short lived annual species such as subterranean clover finishing, but after species like sea barley grass have flowered. It is not possible to specify a particular date as this will depend on seasonal conditions and the region.
- At data capture, ensure that all swathes are flown toward the sun, or alternatively all swathes are flown away from the sun to minimise albedo variation within and between swathes.
- At the time of data capture, collect onground spectral measurements of reference objects (vegetation, soils, built infrastructure and bright and dark targets) with a full range spectrometer to improve atmospheric correction of imagery and potentially provide some reference spectra.
- Collect ground truth data for geo-rectifying, training and testing the image classification. It is important that sufficient validation data is collected to ensure results of image analysis can be used with confidence. The number of validation points will depend on whether a binomial or multi-variate classification is proposed. An experienced biometrician should be engaged to design a sampling system.
- Check the atmospheric correction applied by the vendor and investigate alternative algorithms.
- Conduct a preliminary investigation of the spectral response within image data and identify the critical land cover classes within the image.
- Perform an MNF transform of the image.
- Geo-rectify the image.
- Develop reference spectra library based on ground data.
- Apply the MTMF algorithm to the un-rectified MNF transformed image.
- Create MF score/infeasibility ratios for all relevant land cover classes/reference spectra identified within the image.
- Investigate the ratio scores for critical land cover classes/reference spectra.
- Implement a rule classifier or maximum likelihood classifier based on the MF score/infeasibility ratios.
- Test the output against independent ground data.
- Refine the classification based on the MF score/infeasibility ratios if required.

If using multiple swathes to provide a classification at sub-catchment scale or greater, the most efficient and accurate way is to create a mosaic prior to analysis. Calibration of hyperspectral swathes to a base swathe is a complex operation and needs further investigation before any landscape scale mapping programs are commissioned. Software and algorithms have been developed for this task, but the recommendation is to fully test the utility of these processes before engaging in a large scale project using multiple hyperspectral swathes. An alternative is to treat each swathe individually, but this would require much more ground data and processing time.

Results attained in this research suggest that future data acquisition for mapping areas of saline soil at a landscape scale (with a hyperspectral sensor comparable with the HyMap sensor in terms of spectral resolution and SNR) could be made with a spatial resolution of 10 m without affecting the accuracy. The reduced spatial resolution means increased swathe width, which should also reduce data acquisition costs as less flightlines (and time) would be needed to cover a specified area. Spatial resolution of 10 m would provide data compatible with the spatial accuracy of the existing DPI/DSE soil salinity database, where previous data has been collected at 1:25 000 scale.

8 Conclusion

The results achieved in this study demonstrate that it is possible to map saline and non-saline soil using hyperspectral imagery to a level of accuracy greater than 80% +/- 10% with 90% confidence within a single image swathe. Several classification algorithms were able to achieve this level of accuracy, but the most promising results were achieved using the MTMF algorithm. This sub-pixel algorithm is capable of detecting the abundance of specified materials within a pixel. There is potential to improve on the accuracy and detail achieved using this approach by undertaking a more detailed analysis of the land cover classes identified on a per pixel basis and application of a more sophisticated second stage classifier, but this requires further investigation. The spatial resolution needed to map soil salinity was also investigated and results demonstrated that pixel resolutions of either 15 m or 30 m were able to achieve similar accuracy to that achieved using 3 m spatial resolution.

In the course of this project, several issues that currently limit the implementation of this technology at a larger scale were identified, the prime impediment being the ability to calibrate airborne hyperspectral swathes to a base image. It was outside the scope of this project to investigate this complex issue, but it is something that cannot be ignored if this type of data is to be used to best advantage across sub-catchment areas or larger. Until satellite based systems can match the performance of airborne hyperspectral sensors, the only economic way of utilising this data may be if multiple outcomes could be achieved with the same dataset i.e. grassland mapping, soil salinity, wetland condition and extent all mapped with the same dataset. Failing this, landscape scale analysis based on hyperspectral sensors may have to wait until cheaper data from satellite based sensors can be obtained with satisfactory spatial, spectral and radiometric resolutions and signal to noise ratios as well as regular data capture programs. However, as field based methods of monitoring are becoming less affordable, research in this area should be continued to provide the impetus for the development of new sensors. The skills developed in the course of this project provide a good base to further develop this technology for mapping soil salinity at landscape scale and other vegetation and soil related applications of hyperspectral data for natural resource management.

References

Ahn CW, Baumgardner MF, Biehl LL (1999) Delineation of soil variability using geostatistics and fuzzy clustering analyses of hyperspectral data. *Soil Science Society of America Journal* **63**, 142-150.

Al Saifi MM, Qari MYHT (1996) Application of Landsat Thematic Mapper data in sabkha studies at the Red Sea coast. *International Journal of Remote Sensing* **17**, 527-536.

Allan MJ (1996) Method for field assessment of dryland salinity in Victoria. Technical Report No. 34. Centre for Land Protection Research, Department of Natural Resources and Environment, Victoria.

Bajcsy P, Groves P (2004) Methodology for hyperspectral band selection. *Photogrammetric Engineering & Remote Sensing* **70**, 793-802.

Bedidi A, Cervelle B, Madeira J, Pouget M (1992) Moisture effects on visible spectral characteristics of lateritic soils. *Soil Science* **153**, 129-141.

Ben-Dor E, Goldlshleger N, Benyamini Y, Agassi M, Blumberg DG (2003) The spectral reflectance properties of soil structural crusts in the 1.2- to 2.5-microns spectral region. *Soil Science Society of America Journal* **67**, 289-299.

Ben-Dor E, Irons JA, Epema A (1999) Soil spectroscopy. In 'Remote Sensing for the Earth Sciences: Manual of Remote Sensing, 3rd edition'. (Ed. A Renz) pp. 111-189. (John Wiley: New York)

Bennetts D, Webb JA, Gray CM (2003) Distribution of Plio-Pleistocene basalts and regolith around Hamilton, western Victoria, and their relationship to groundwater recharge and discharge. In *Advances in Regolith*. (Ed. IC Roach) pp. 11-15. (CRC LEME)

Boardman J (1989) Inversion of imaging spectrometer data using singular value decomposition. In 'IGARSS'89'. Vancouver

Bowers SA, Hanks RJ (1965) Reflection of radiant energy from soils. *Soil Science* **100**, 130-138.

Chabrillat S, Goetz AFH, Krosley L, Olsen HW (2002) Use of hyperspectral images in the identification and mapping of expansive clay soils and the role of spatial resolution. *Remote Sensing of Environment. Elsevier Science Inc., New York, USA* **82**, 431-445.

Clark RN (1999) Spectroscopy of rocks and minerals, and principles of spectroscopy. In *Remote Sensing for the Earth Sciences: Manual of Remote Sensing*, 3rd edition'. (Ed. AN Renz) pp. 3-58. (John Wiley: New York)

Cochrane MA (2000) Using vegetation reflectance variability for species level classification of hyperspectral data. *International Journal of Remote Sensing* **21**, 2075-2087.

Cocks T, Jenssen R, Stewart A, Wilson I, Shields T (1998) The Hymap airborne hyperspectral sensor: the system, Calibration and performance. In '1st EARSEL workshop on Imaging Spectroscopy'. Zurich

Congalton RG, Green K (1998) *Assessing the Accuracy of Remotely Sensed Data: Principles and Practices.* (Lewis)

Csillag F, Pasztor L, Biehl L (1993) Spectral band selection for the characterization of salinity status of soils. *Remote Sensing of Environment* **43**, 231-242.

Dehaan R, Taylor GR (2003) Image-derived spectral endmembers as indicators of salinisation. *International Journal of Remote Sensing. Taylor & Francis Ltd, Abingdon, UK* **24**, 775-794.

Dehaan RL, Taylor GR (2002) Field-derived spectra of salinized soils and vegetation as indicators of irrigation-induced soil salinization. *Remote Sensing of Environment* **80**, 406-417.

Dwivedi RS, Sreenivas K (1998) Delineation of salt affected soils and waterlogged areas in the Indo-Gangetic plains using IRS-1C LISS-III data. *International Journal of Remote Sensing* **19**, 2739-2751.

Furby S, Clark R (2003) Monitoring land use and condition change using remotely sensed data. Salinity mapping qand monitoring in the Wimmera River region. CSIRO Mathematical and Information Sciences.

Furby SL, Wallace JF, Caccetta P, Wheaton GA (1995) Detecting and Monitoring Salt-affected Land. A report from the LWRRDC project, Detecting and Monitoring Changes in Land Condition Through Time using Remotely Sensed Data. CSIRO Mathemetical and Information Sciences

Glenn NF, Mundt JT, Weber KT, Prather TS, Lass LW, Pettingill J (2005) Hyperspectral data processing for repeat detection of small infestations of leafy spurge. *Remote Sensing of Environment* **95**, 399-412.

Gonzalez RC, Wintz P (1987) *Digital Image Processing*, 2nd Edition. (Addison-Wesley)

Hill SR (1990) Land classification using remote sensing and geographic information systems: A salinity case study. Department of Conservation and Environment.

Jensen JR (1996) *Introductory digital image processing. A remote sensing perspective*. (Prentice Hall: New Jersey)

LCC (1978) Report on the South-Western Area, District 2. Land Conservation Council, Victoria.

Leone AP, Sommer S (2000) Multivariate analysis of laboratory spectra for the assessment of soil development and soil degradation in the southern Apennines (Italy). *Remote Sensing of Environment* **72**, 346-359.

Matthews C, Clark R, Callinan L (2006) Spectral Discrimination of Southern Victorian Salt Tolerant Vegetation. In *Advances in Data Mining – Applications in Medicine, Web Mining, Marketing, Image and Signal Mining*, LNAI. Heidelberg. (Ed. P.Perner) pp. 389-403. (Springer Verlag)

McCloy KR (1995) Interaction of radiation with matter. In *Resource management information systems: processes and practice* pp. 28-44. (Taylor and Francis: London)

McDonald RC, Isbell RF, Speight JG, Walker J, Hopkins MS (1990) *Australian soil and land survey field handbook* (second edition). (Inkata Press: Melbourne)

Metternicht GI, Zinck JA (2003) Remote sensing of soil salinity: Potentials and constraints. *Remote Sensing of Environment* **85**, 1-20.

NLWRA (2000) Australian Dryland Salinity Assessment 2000: Extent, impact, processes and management options. National Land and Water Resources Audit, Canberra.

Price JC (1992) Variablility of high resolution crop reflectance spectra. *International Journal of Remote Sensing* **14**, 2593-2610.

RSI (2000) 'ENVI user's guide. ENVI version 3.4.' (Research Systems Incorporated: Boulder, CO)

RSI (2006) ENVI Version 4.2 Online Help. (Research Systems Incorporated: Boulder, CO)

Ryan S, Lewis M (n.d.) Mapping soil using high resolution airborne imagery, Barossa Valley, SA.

Schiefer S, Hostert P, Damm A (2006) Correcting brightness gradients in hyperspectal data from urban areas. *Remote Sensing of Environment* **in press**.

Schmidt KS (2003) Hyperspectral remote sensing of vegetation species distribution in a saltmarsh. Ph.D. Thesis Wageningen University, The Netherlands.

Schmidt KS, Skidmore AK (2003) Spectral discrimination of vegetation types in a coastal wetland. *Remote Sensing of the Environment* **85**, 92-108.

Shippert P (2004) Why use hyperspectral imagery? *Photogrammetric Engineering & Remote Sensing* **70**, 377-380.

Spies B, Woodgate P (2005) Salinity Mapping Methods in Australian Context. Department of Environment and Heritage; and Agriculture, Fisheries and Forestry., Canberra.

Stoner ER, Baumgardner MR (1980) Physiochemical, site, and bidirectional reflectance factor characteristics of uniformly moist soils. Purdue Univarsity, West Lafayette, IN.

US Naval Observatory AAD (2006) Sun or Moon azimuth table for one day.

Van Der Meer F, De Jong SM (2003) *Image spectrometry. Basic principles and prospective applications.* (Kluwer: Dordrecht/ Boston/ London)

Wu Y, Chen J, Wu X, Tian Q, Ji J, Qin Z (2005) Possibilities of reflectance spectroscopy for the assessment of contaminant elements in suburban soils. *Applied Geochemistry* **20**, 1051-1059.

Zink JA (2001) Monitoring salinity from remote sensing data. *Proceedings of the 1st Workshop of the EARSel Special Interest Group on Remote Sensing for Developing Countries*. Ghent University, Belgium

Appendices

Appendix 1 Summary of sun azimuth and sensor heading for each HyMap swathe.

Swathe number	Sun azimuth (degrees)	Sensor heading (degrees)	Difference between sun azimuth and sensor heading (degrees)
dpi01	274.0	273	1
dpi02	275.0	92	183
dpi03	275.5	273	2.5
dpi04	277.5	62	215.5
dpi05	278.7	248	30.7
dpi06	280.0	62	218
dpi07	284.9	357	72.1
dpi08	287.3	181	106.3
dpi09	287.3	0	72.3
dpi10	282.7	202	80.7
dpi11	282.7	82	200.7
dpi12	289.6	178	111.6

Appendix 2 Method for collecting soil samples

Step 1

A measuring tape is laid out on the bare soil area. Bare areas were selected on the basis of largest patches of bare earth, or a concentration of bare earth was selected. This area of sampling was defined from a 1 metre radius.

Step 2

Two soil cores are placed within the selected defined sampling area for the bare patch. Soil surfaces generally free from significant surface organic matter (humus) were selected. Cores were then hammered into the ground using a steel post driver and block of hardwood. Soil cores were then wrapped in cling film and refrigerated to preserve moisture contents for future analysis.

Step 3

Disturbed samples were collected from the defined sampling area. Soil was collected using a spatula to obtain a sample from the surface (1-2 cm). This was done to select soil most closely associated with spectral properties collected by the HyMap sensor rather than deeper soil that may have distinctly different properties (chemical, physical and spectral) than the surface. The disturbed sample was then examined for properties including soil colour, field pH, field texture and presence of carbonates as fine earths.

Step 4

The site was then geo-referenced using a differential GPS for future reference of these saline sites.

Appendix 3 Soil sample preparation

The soil samples were ground in an agate mortar and pestle then pressed into aluminium sample holders for X-ray diffraction analysis. XRD patterns were recorded with a Philips PW1800 microprocessor-controlled diffractometer using Co Kα radiation, variable divergence slit, and graphite monochromator. The diffraction patterns were recorded in steps of 0.05° 2θ with a 1.0 second counting time per step, and logged to data files on an IBM-compatible PC for analysis using XPLOT data analysis program. Results are provided in the table below along with an example of the XRD plot.

Sample	Mineralogical composition
4-2	Dominant quartz, minor smectite (montmorillonite), trace albite, microcline, calcite and anatase
4-5	Dominant quartz, minor smectite (montmorillonite) and kaolin, trace albite, microcline, goethite, possible ilmenite and anatase
4-6	Dominant quartz, minor smectite (montmorillonite), kaolin and maghemite, trace albite, microcline, goethite and/or hematite, ilmenite and anatase
5-4	Dominant quartz, minor halite and smectite (montmorillonite), trace kaolin, albite, microcline, and anatase
6-1	Co-dominant quartz and amorphous material (organic?), minor halite, trace smectite (montmorillonite), kaolin, albite, microcline, and anatase
6-2	Dominant quartz, minor halite and smectite (montmorillonite), trace kaolin, possible Mg-calcite, albite, microcline, and anatase
6-4	Dominant quartz, minor halite and smectite (montmorillonite), trace kaolin, albite, microcline, and anatase
7-1	Dominant quartz, minor halite and smectite (montmorillonite), trace kaolin, albite and microcline
7-2	Dominant quartz, minor halite and smectite (montmorillonite), trace possible Mg-calcite, kaolin, albite, microcline, possible ilmenite and anatase
7-4	Dominant quartz, minor halite and smectite (montmorillonite), trace possible Mg-calcite, kaolin, albite, microcline, ilmenite and anatase

*Dominant (>60%), co-dominant (sum of phases >60%), sub-dominant (20-60%), minor (5-20%), trace (<5%).

Sample XRD plot

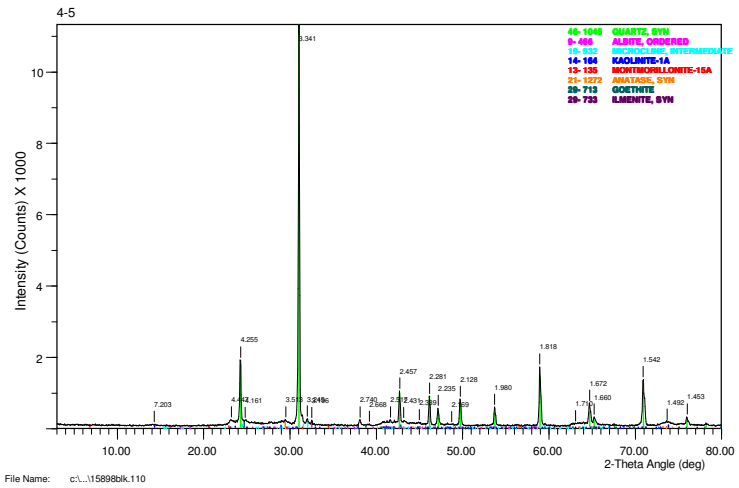

Appendix 4 Soil analyses

	Sample number				
	4-1	4-2	4-3	4-4	4-5
Chemical analysis					
pH (H_2O)	7.4	7.6	7.1	7.0	4.7
pH ($CaCl_2$)	7.3	7.5	7.1	6.8	4.5
$EC_{1:5}$ (dS/m)	4.9	3.1	7.5	11.0	1.3
T.S.S. (%w/w)	1.50	0.92	2.20	3.30	0.39
Cl (mg/kg)		90			110
XRD analysis					
(major minerals)		quartz albite microcline montmorillonite anatase calcite			quartz albite microcline kaolinite montmorillonite anatase goethite ilmenite
Moisture content (% gravimetric)	19.15		18.81	16.68	8.29
Field analysis					
pH	6.5	7.5-8.0	7.5-8.0	7.5	4.5
Texture	Light clay, silty	Light clay, silty	Light clay, silty	Medium heavy clay	Clay loam
Munsell colour	2.5Y4/1	2.5Y5/1	2.5Y3/1	10YR3/1	10YR4/2
Effervescence of carbonate in fine earth	Moderately calcareous	Highly calcareous	Slightly-moderately calcareous	Nil	Nil

Appendix 4 (continued)

	Sample number				
	4-6	5-1	5-2	5-3	5-4
Chemical analysis					
pH (H_2O)	4.6	7.0	6.9	7.2	7.6
pH ($CaCl_2$)	4.4	6.9	6.9	7.2	7.5
$EC_{1:5}$ (dS/m)	1.1	26.0	30.0	19.0	12.0
T.S.S. (%w/w)	0.33	7.70	8.90	5.70	3.60
Cl (mg/kg)					24 000
XRD analysis					
(major minerals)	quartz albite microcline kaolinite montmorillonite anatase goethite ilmenite hematite maghemite				quartz albite microcline kaolinite montmorillonite anatase halite
Moisture content (% gravimetric)	7.67	17.68	20.66	17.14	23.02
Field analysis					
pH	4.0-4.5	6.0-6.5	6.5-7.0	7.0-8.0	7.0-7.5
Texture	Clay loam	Light clay	Light clay	Light clay	Light clay
Munsell colour	10YR4/2	2.5Y3/1	10YR3/1	10YR3/1	10YR3/1
Effervescence of carbonate in fine earth	Nil	Nil	Nil	Nil	Nil

Appendix 4 (continued)

	Sample number			
	6-1	6-2	6-3	6-4
Chemical analysis				
pH (H_2O)	6.2	8.1	6.5	7.0
pH ($CaCl_2$)	6.0	8.1	6.5	6.9
$EC_{1:5}$ (dS/m)	28.0	21.0	24.0	22.0
T.S.S. (%w/w)	8.30	6.20	7.10	6.50
Cl (mg/kg)				46 000
XRD analysis				
(major minerals)	quartz albite microcline kaolinite montmorillonite anatase halite	quartz albite microcline kaolinite montmorillonite anatase halite calcite		quartz albite microcline kaolinite montmorillonite anatase halite
Moisture content (% gravimetric)	23.93	26.56	23.77	23.61
Field analysis				
pH	5.0	8.5-9.0	6.0-6.5	6.0-6.5
Texture	Loam	Light clay	Light clay	Light clay
Munsell colour	10YR3/1	2.5Y5/2	7.5YR3/1	10YR4/1
Effervescence of carbonate in fine earth	Nil	Moderately calcareous	Nil	Nil

Appendix 4 (continued)

	Sample number			
	7-1	7-2	7-3	7-4
Chemical analysis				
pH (H_2O)	8.1	7.0	7.4	6.4
pH ($CaCl_2$)	8.0	6.8	7.4	6.3
$EC_{1:5}$ (dS/m)	24.0	11.0	29.0	19.0
T.S.S. (%w/w)	7.10	3.30	8.60	5.70
Cl (mg/kg)				48 000
XRD analysis				
(major minerals)	quartz albite microcline kaolinite montmorillonite halite	quartz albite microcline kaolinite montmorillonite anatase halite ilmenite calcite		quartz albite microcline kaolinite montmorillonite anatase halite ilmenite calcite
Moisture content (% gravimetric)	21.96	35.35	27.48	27.27
Field analysis				
pH	7.5	8.0	6.5-7.0	5.0-5.5
Texture	Medium heavy clay	Light medium clay	Medium clay	Medium clay
Munsell colour	10YR3/1	10YR3/1	10YR3/1	7.5YR3/1
Effervescence of carbonate in fine earth	Nil	Nil	Nil	Nil

Appendix 5 Image classification results

Maximum Likelihood Supervised Classification

The Maximum Likelihood algorithm was applied both to reflectance data (Tables E.1 and E.2) and MNF transformed data (Tables E.3 and E.4) using the reference spectra libraries collected from GPS surveys and landholder knowledge.

Table E.1 Error matrix for the maximum likelihood supervised classification based on HyMap reflectance data and using the reference spectra libraries collected from GPS surveys and landholder knowledge.

	Ground truth saline point	Ground truth non-saline point	Total count
Saline image class	84	25	109
Non-saline image class	15	110	125
Unclassified image class	12	20	32
Total count	111	155	266

The overall classification accuracy including unclassified pixels as not correctly identified = 194/266 = 73%.

Table E.2 The producer's and user's accuracy for the maximum likelihood supervised classification based on HyMap reflectance data and using the reference spectra libraries collected from GPS surveys and landholder knowledge.

	Producer's accuracy		User's accuracy	
Saline soil	84/111	76%	84/109	77%
Non-saline soil	110/155	71%	110/125	85%

Table E.3 Error matrix for the maximum likelihood supervised classification based on MNF transformed reflectance data and using the MNF transformed reference spectra libraries collected from GPS surveys and landholder knowledge.

	Ground truth saline point	Ground truth non-saline point	Total count
Saline image class	87	13	100
Non-saline image class	6	133	139
Unclassified image class	18	9	27
Total count	111	155	266

The overall classification accuracy including unclassified pixels as not correctly identified = 220/266 = 83%.

Table E.4 The producer's and user's accuracy for the maximum likelihood supervised classification based on MNF transformed reflectance data and using the MNF transformed reference spectra libraries collected from GPS surveys and landholder knowledge.

	Producer's accuracy		User's accuracy	
Saline soil	87/111	78%	87/100	87%
Non-saline soil	133/155	86%	133/139	96%

Spectral Angle Mapper (SAM)
The SAM algorithm was run on the reflectance image using various reference spectra and classification parameters. The SAM algorithm was also run on MNF transformed data using reference spectra collected from field surveys and landholder knowledge, with no SAM threshold set. Results for each classification are listed in tables E.5 – E.14.

1 SAM run using endmembers identified from the PPI image and applied to the reflectance image with SAM threshold = 0.1 radians

Table E.5 Error matrix for the SAM classification (threshold = 0.1 radians) based on HyMap reflectance data and using endmembers identified via the PPI algorithm.

	Ground truth saline point	Ground truth non-saline point	Total count
Saline image classes (13, 17, 19, 26)	33	20	53
Non-saline image classes	36	93	129
Unclassified image classes(0)	42	42	84
Total count	111	155	266

This gave an overall accuracy of 126/266 = 47% if unclassified points are counted as wrong.

Table E.6 The producer's and user's accuracy for the SAM classification (threshold = 0.1 radians) based on HyMap reflectance data and using endmembers identified via the PPI algorithm.

	Producer's accuracy		User's accuracy	
Saline soil	33/111	30%	33/53	62%
Non-saline soil	93/155	60%	93/129	72%

2 SAM run using reference spectra derived from field survey and landholder input and applied to the reflectance image, SAM threshold = 0.1 radians

Table E.7 Error matrix for the SAM classification (threshold = 0.1 radians) based on HyMap reflectance data and using the reference spectra libraries collected from GPS surveys and landholder knowledge.

	Ground truth saline point	Ground truth non-saline point	Total count
Saline image classes (1-14)	76	17	93
Non-saline image classes (15-51)	21	137	158
Unclassified image classes(0)	14	1	15
Total count	111	155	266

This gave an overall accuracy of 213/266 = 80% if unclassified points are counted as wrong.

Table E.8 The producer's and user's accuracy for the SAM classification (threshold = 0.1 radians)based on HyMap reflectance data and using the reference spectra libraries collected from GPS surveys and landholder knowledge.

	Producer's accuracy		User's accuracy	
Saline soil	76/111	68%	76/93	82%
Non-saline soil	137/155	88%	137/158	87%

3 SAM run using reference spectra derived from field survey and landholder input and applied to the reflectance image, with nil SAM threshold set

Table E.9 Error matrix for the SAM classification (nil threshold set) based on HyMap reflectance data and using the reference spectra libraries collected from GPS surveys and landholder knowledge.

	Ground truth saline point	Ground truth non-saline point	Total count
Saline image classes (1-14)	87	17	104
Non-saline image classes (15-51)	21	138	159
Unclassified image classes(0)	3	0	3
Total count	111	155	266

This gave an overall accuracy of 225/266 = 85% if unclassified points are counted as wrong.

Table E.10 The producer's and user's accuracy for the SAM classification (nil threshold set)based on HyMap reflectance data and using the reference spectra libraries collected from GPS surveys and landholder knowledge.

	Producer's accuracy		User's accuracy	
Saline soil	87/111	78%	87/104	84%
Non-saline soil	138/155	89%	138/159	87%

4 SAM run using laboratory measured vegetation spectra as the reference spectra and applied to the reflectance image, with nil SAM threshold set

Reference spectra derived from vegetation spectra collected using a VisNIR spectrometer in laboratory conditions with controlled illumination.

Table E.11 Error matrix for the SAM classification (nil threshold set) on HyMap reflectance data using the vegetation laboratory spectra as the reference spectra.

	Ground truth saline point	Ground truth non-saline point	Total count
Saline image classes (9-11, 32-42, 55-59)	39	39	78
Non-saline image classes (2-8, 12-31, 43-54, 60-63)	69	116	185
Unclassified image classes (0)	3	0	3
Total count	111	155	266

This gave an overall accuracy of 155/266 = 58% if unclassified points are counted as wrong.

Table E.12 The producer's and user's accuracy for the SAM classification (nil threshold set) on HyMap reflectance data using the vegetation laboratory spectra as the reference spectra.

	Producer's accuracy		User's accuracy	
Saline soil	39/111	35%	39/78	50%
Non-saline soil	116/155	75%	116/185	63%

5 SAM run using reference spectra derived from field survey and landholder input and applied to a 25 band MNF transformed image, with nil SAM threshold set

Table E.13 Error matrix for the SAM classification (nil threshold set) on 25 band MNF transformed reflectance data using the reference spectra libraries collected from GPS surveys and landholder knowledge.

	Ground truth saline point	Ground truth non-saline point	Total count
Saline image classes (1-13 & 39)	90	6	96
Non-saline image classes (14-38, 40-51	8	123	131
Unclassified image classes (0)	13	26	39
Total count	111	155	266

The overall accuracy was 213/266 = 80% if unclassified points are counted as wrong.

Table E.14 The producer's and user's accuracy for the SAM classification (nil threshold set) on 25 band MNF transformed reflectance data using the reference spectra libraries collected from GPS surveys and landholder knowledge.

	Producer's accuracy		User's accuracy	
Saline soil	90/111	81%	90/96	94%
Non saline soil	123/155	79%	123/131	94%

Spectral Feature Fitting (SFF)

Visual assessment of the SFF algorithm results indicated there was little ability to discriminate between reference spectra in the image data. As a result, the SFF outputs were not tested against the ground validation data.

Mixture Tuned Matched Filtering (MTMF)

All MTMF classifications were run on MNF transformed data using various reference spectra. Matched filter/ infeasibility MTMF ratios were produced for set of reference spectra. Each ratio set was then run through either a maximum likelihood algorithm or simple rule classifier algorithm to produce a saline or non-saline classification for the trial area. The results for each classification are listed in Tables E.15-E.24.

1 MTMF algorithm run using MNF transformed reference spectra collected from field surveys and landholder knowledge and soil spectra for wet and dry undisturbed samples measured in the laboratory.

a MTMF matched filter/ infeasibility ratios classified using maximum likelihood algorithm (with threshold value = zero) using training areas generated from field surveys and landholder knowledge

Table E.15 Error matrix for the MTMF algorithm run using MNF transformed reference spectra collected from field surveys and landholder knowledge and soil spectra measured in the laboratory. MTMF matched filter/ infeasibility ratios classified using a maximum likelihood algorithm (threshold = 0), using training areas generated from field surveys and landholder knowledge.

	Ground truth saline point	Ground truth non-saline point	Total count
Saline image classes (1, 27, 37)	95	12	107
Non-saline image classes (2-26, 28-36)	14	143	157
Unclassified image classes(0)	2	0	2
Total count	111	155	266

This gave an overall accuracy of 238/266 = 89% if unclassified points are counted as wrong.

Table E.16 The producer's and user's accuracy for the MTMF algorithm run using MNF transformed reference spectra collected from field surveys and landholder knowledge and soil spectra measured in the laboratory. MTMF matched filter/ infeasibility ratios classified using a maximum likelihood algorithm (threshold = 0), using training areas generated from field surveys and landholder knowledge.

	Producer's accuracy		User's accuracy	
Saline soil	95/111	85%	95/107	89%
Non-saline soil	143/155	92%	143/157	91%

b MTMF matched filter/ infeasibility ratios classified using a rule classifier with no threshold set.

The accuracy assessment was as follows

Table E.17 Error matrix for the MTMF algorithm run using MNF transformed reference spectra collected from filed surveys and landholder knowledge and soil spectra measured in the laboratory. MTMF matched filter/ infeasibility ratios classified using a rule classifier (nil threshold set).

	Ground truth saline point	Ground truth non-saline point	Total count
Saline image classes (1-14, 43, 44, 46-54, 56-61)	92	10	102
Non-saline image classes (15-42, 45, 55)	16	145	161
Unclassified image classes(0)	3	0	3
Total count	111	155	266

This gave an overall accuracy of 237/266 = 89% if unclassified points are counted as wrong.

Table E.18 The producer's and user's accuracy for the MTMF algorithm run using MNF transformed reference spectra collected from field surveys and landholder knowledge and soil spectra measured in the laboratory. MTMF matched filter/ infeasibility ratios classified using a rule classifier (nil threshold set).

	Producer's accuracy		User's accuracy	
Saline soil	92/111	83%	92/102	90%
Non-saline soil	145/155	94%	145/161	90%

2 Run MTMF using MNF transformed reference spectra collected from salt-tolerant and salt-sensitive vegetation measured in the laboratory with a Visible and Near Infrared (VNIR) spectrometer

a. MTMF matched filter/ infeasibility ratios classified using maximum likelihood classification (with threshold value = zero) using training areas generated from field surveys and landholder knowledge

Table E.19 Error matrix for the MTMF classification using MNF transformed reference spectra collected from salt-tolerant and salt-sensitive vegetation in the laboratory with a Visible and Near Infrared (VNIR) spectrometer. MTMF matched filter/ infeasibility ratios classified using a maximum likelihood classifier (threshold = 0), using training areas generated from field surveys and landholder knowledge.

	Ground truth saline point	Ground truth non-saline point	Total count
Saline image classes (1, 27, 37)	44	10	54
Non-saline image classes (2-26, 28-36)	67	145	212
Unclassified image class (0)	0	0	0
Total count	111	155	266

This gave an overall accuracy of 189/266 = 71% if unclassified points are counted as wrong.

Table E.20 The producer's and user's accuracy for the MTMF classification using MNF transformed reference spectra collected from salt-tolerant and salt-sensitive vegetation in the laboratory with a Visible and Near Infrared (VNIR) spectrometer. MTMF matched filter/ infeasibility ratios classified using a maximum likelihood classifier (threshold = 0), using training areas generated from field surveys and landholder knowledge.

	Producer's accuracy		User's accuracy	
Saline soil	44/111	40%	44/54	80%
Non saline soil	145/155	94%	145/212	68%

b. MTMF matched filter/ infeasibility ratios classified using a rule classifier with no threshold set.

Table E.21 Error matrix for the MTMF classification using MNF transformed reference spectra collected from salt-tolerant and salt-sensitive vegetation in the laboratory with a Visible and Near Infrared (VNIR) spectrometer. MTMF matched filter/ infeasibility ratios combined using a rule classifier (nil threshold set).

	Ground truth saline point	Ground truth non-saline point	Total count
Saline image classes (9-11, 32-42, 55-59)	61	54	105
Non-saline image classes (1-8, 12-31, 43-54, 60-63)	47	101	148
Unclassified (0)	3	0	3
Total count	111	155	266

This gave an overall accuracy of 162/266 = 61% if unclassified points are counted as wrong.

Table E.22 The producer's and user's accuracy for the MTMF classification using MNF transformed reference spectra collected from salt-tolerant and salt-sensitive vegetation in the laboratory with a Visible and Near Infrared (VNIR) spectrometer. MTMF matched filter/ infeasibility ratios combined using a rule classifier (nil threshold set).

	Producers accuracy		Users accuracy	
Saline soil	61/111	55%	61/115	53%
Non-saline soil	101/155	65%	101/148	68%

3 Run MTMF algorithm using MNF transformed endmembers generated via the PPI algorithm

a MTMF Matched filter/ infeasibility ratios classified using maximum likelihood classification (with threshold value = zero) using training areas generated from field surveys and landholder knowledge

Table E.23 Error matrix for the MTMF algorithm run using MNF transformed endmembers generated via the PPI algorithm. MTMF matched filter/ infeasibility ratios classified using a maximum likelihood classifier (threshold = 0), using training areas generated from field surveys and landholder knowledge.

	Ground truth saline point	Ground truth non-saline point	Total count
Saline image classes (1, 27, 37)	75	6	81
Non-saline image classes (2-26, 28-36)	34	149	183
Unclassified image classes (0)	2	0	2
Total count	111	155	266

This gave an overall accuracy of 224/266 = 84% if unclassified points are counted as wrong.

Table E.24 The producer's and user's accuracy using MNF transformed endmembers generated via the PPI algorithm. MTMF matched filter/ infeasibility ratios classified using a maximum likelihood classifier (threshold = 0), using training areas generated from field surveys and landholder knowledge.

	Producer's accuracy		User's accuracy	
Saline soil	75/111	68%	75/81	93%
Non saline soil	149/155	96%	149/183	81%

Spatial Resampling

The reflectance data was resampled from 3 m pixels to produce images with 15 m and 30 m pixels. Both sets of resampled data were MNF transformed and the MTMF algorithm was applied to each image using MNF transformed reference spectra collected from field surveys and landholder knowledge and soil spectra for wet and dry undisturbed samples measured in the laboratory. For both 15 m and 30 m pixel resolution images matched filter/infeasibility MTMF ratios were produced for each reference spectra. Each ratio set was then run through a simple rule classifier algorithm to produce a saline or non-saline classification for the trial area. The results for the 15 m and 30 m pixel resolution images are listed in Tables E.25 to E.28.

1. MTMF algorithm run on 15 m spatial resolution using MNF transformed reference spectra collected from field surveys and landholder knowledge and soil spectra for wet and dry undisturbed samples measured in the laboratory.

Table E.25. Error matrix for the MTMF algorithm run on the 15m pixel resolution image using MNF transformed reference spectra collected from field surveys and landholder knowledge and soil spectra measured in the laboratory. MTMF matched filter/ infeasibility ratios classified using a rule classifier (nil threshold set).

	Ground truth saline point	Ground truth non-saline point	Total count
Saline image classes (1-12, 38, 51, 52, 54-62, 64-69)	87	11	98
Non-saline image classes (13-37, 39-50, 53, 63)	12	139	151
Unclassified image classes (157)	9	4	13
Total count	108	154	262

This gave an overall accuracy of 226/262 = 86% if unclassified points are counted as wrong.

Table E.26 The producer's and user's accuracy for the MTMF algorithm run on the 15m pixel resolution image using MNF transformed reference spectra collected from field surveys and landholder knowledge and soil spectra measured in the laboratory. MTMF matched filter/ infeasibility ratios classified using a rule classifier (nil threshold set).

	Producer's accuracy		User's accuracy	
Saline soil	87/108	81%	87/98	89%
Non-saline soil	139/154	90%	139/151	92%

2. MTMF algorithm run on 30m spatial resolution using MNF transformed reference spectra collected from field surveys and landholder knowledge and soil spectra for wet and dry undisturbed samples measured in the laboratory.

Table E.27 Error matrix for the MTMF algorithm run on the 30m pixel resolution image using MNF transformed reference spectra collected from filed surveys and landholder knowledge and soil spectra measured in the laboratory. MTMF matched filter/ infeasibility ratios classified using a rule classifier (nil threshold set).

	Ground truth saline point	Ground truth non-saline point	Total count
Saline image classes (1-12, 38, 50, 51, 53-61, 63-68)	80	15	95
Non-saline image classes (13-37, 39-49, 52, 62)	19	137	156
Unclassified image classes(241)	10	2	12
Total count	109	154	263

This gave an overall accuracy of 217/263 = 83% if unclassified points are counted as wrong.

Table E.28 The producer's and user's accuracy for the MTMF algorithm run on the 30 m pixel resolution image using MNF transformed reference spectra collected from field surveys and landholder knowledge and soil spectra measured in the laboratory. MTMF matched filter/ infeasibility ratios classified using a rule classifier (nil threshold set).

	Producer's accuracy		User's accuracy	
Saline soil	80/109	73%	80/95	84%
Non-saline soil	137/154	89%	137/156	88%